THE FATE AND TRANSPORT OF ANTHROPOGENIC HALOGENATED VOLATILE ORGANIC COMPOUNDS (HVOCS) IN GALVESTON BAY, TX

A Thesis

by

GARRETT XAVIER WALSH

Submitted to the Office of Graduate and Professional Studies of
Texas A&M University
in partial fulfillment of the requirements for the degree of

MASTER OF SCIENCE

Chair of Committee,	Shari Yvon-Lewis
Co-Chair of Committee,	Yina Liu
Committee Members,	Peter Santschi
Head of Department,	Shari Yvon-Lewis

May 2021

Major Subject: Oceanography

ABSTRACT

Distribution and transport of anthropogenic halogenated volatile organic carbons (HVOCs) are not well studied in estuary settings. Carbon tetrachloride (CCl_4) and CFC-11 are banned substances under the Montreal Protocol, and can potentially be used as tracers for contamination sources within estuaries. Chloroform ($CHCl_3$) and perchloroethylene (PCE) have many current sources, such as wastewater outfalls and dry cleaner waste. Loss of these HVOCs in surface waters of estuaries is presumed to be mainly through sea-to-air flux due to their volatility and long lifetimes in aerobic waters.

Galveston Bay is heavily influence by anthropogenic activity and forcing events in Texas. Measurements of CCl_4, CFC-11, $CHCl_3$, and PCE were made in Galveston Bay in March, June, September, and November 2019. In March, a large chemical plant fire at the Intercontinental Terminals Company (ITC) in Deer Park, TX released an unknown quantity and composition of liquid into Galveston Bay via the Houston Ship Channel. In September, Tropical Storm Imelda released up to 39 inches of rain in the Galveston Bay watershed, potentially leading to a flushing event within the bay.

Elevated concentrations of CCl_4, $CHCl_3$, CFC-11, and PCE were in the Buffalo Bayou, San Jacinto River, and Lower San Jacinto regions for all sampling months, suggesting anthropogenic sources. Within Galveston Bay, the concentrations of anthropogenic HVOCs is similar to Trinity River and Trinity Bay. Modeled loss of each compound within this region suggests that sea-to-air flux is a significant removal process but is unable to fully explain the loss of anthropogenic HVOCs in the surface water. The

impacts of the ITC fire in Deer Park, TX and Tropical Storm Imelda on the concentrations of anthropogenic HVOCs in Galveston Bay and the Houston Ship Channel is unknown without a longer time series.

DEDICATION

For Linda Walsh – may your final words continue to drive me forward, even when I grow weary and tired.

ACKNOWLEDGEMENTS

I would like to thank my advisors Dr. Shari Yvon-Lewis and Dr. Yina Liu for their advice, wisdom, and support while doing this research. I especially want to thank Shari for being a mentor and friend, allowing me to go in any direction I please with my research. And to Yina, thank you for broadening my knowledge and techniques by visiting other labs and trusting me to present your research. I would like to thank my final committee member Dr. Peter Santschi for his insight and input into my research.

I would also like to thank the undergraduates and REU students that have come through the Yvon-Lewis Lab, and made research infinitely more fun. Jeramy Dedrick, thank you for putting up with my insane jokes and laughing no matter what. Best lab partner a man could ask for. Melissa Shugart, thank you for bringing your humor, curiosity, and thirst for scientific knowledge, along with your drive to succeed and to get Gerald working. I am glad to count you amongst my friends. And finally, to Hunter Adams – the long talks we had about multiple topics are only matched by the memes we laughed at. I wish you nothing but the best in life going forward my friend. That's a Texas-sized 10-4 good buddy.

A special thank you goes to my amazing girlfriend Jessica Lowe. Moving thousands of miles with me to achieve my goals, putting up with my long hours and frustrations, and supporting me throughout this process has made it possible for me to do this. I could not have done it without you. Cannot forget Bailey as well – a better dog does not exist. All the treats and pets are yours.

I would finally like to thank my brothers Cameron and Bob for always providing unexpected laughs and advice. We have always supported each other through thick and thin. Let us continue to do so for quite some more time.

CONTRIBUTORS AND FUNDING SOURCES

Contributors

This work was supervised by a thesis committee consisting of co-chairs Professor Shari Yvon-Lews and Professor Yina Liu of the Department of Oceanography at Texas A&M University and Professor Peter Santschi of the Department of Marine Sciences at Texas A&M University-Galveston. All work for the thesis was completed independently by the student.

Funding Sources

Graduate study was supported by the NSF S-STEM scholarship program.

NOMENCLATURE

CCl_4	Carbon Tetrachloride
$CHCl_3$	Chloroform
PCE	Perchloroethylene
CFC	Chlorofluorocarbon
HVOCs	Halogenated volatile organic compounds
HCFCs	Hydrochlorofluorocarbons
GC/MS	Gas Chromatography/Mass Spectrometer
USEPA	United States Environmental Protection Agency
THMs	Trihalomethanes
HFCs	Hydrofluorocarbons
TCE	Trichloroethene
TCEQ	Texas Commission of Environmental Quality
HSC	Houston Ship Channel
ITC	Intercontinental Terminals Company
DO	Dissolved oxygen
DOM	Dissolved organic matter
CDOM	Colored dissolved organic matter
DIC	Dissolved inorganic carbon
PFAS	Per- and polyfluorinated alkyl substances
SIM	Selective ion mode

NOAA	National Oceanic and Atmospheric Administration
SIO	Scripps Institute of Oceanography
UHPW	Ultra high purity water
USGS	United States Geological Survey
PFOA	Perfluorooctanoic acid
PFOS	Perfluorooctanesulfonic acid
6:2 FTS	6:2 fluorotelomer sulfonate
AFFF	Air firefighting foam
PFBS	Perfluorobutanesulfonic acid
TWDB	Texas Water Development Board
AGAGE	Advanced Global Atmospheric Gases Experiment

TABLE OF CONTENTS

Page

LIST OF FIGURES

Page

LIST OF TABLES

Page

1. INTRODUCTION

Halogenated volatile organic compounds (HVOCs) are low molecular weight carbon compounds that contain any combination of fluorine, chlorine, bromine, or iodine. Anthropogenic HVOCs mainly contain fluorine, chlorine, or bromine and have a variety of uses as coolants, adhesives, lubricants, aerosol propellants, and many others (Doherty, 2000). The inherent volatility and inert nature of anthropogenic HVOCs led to the depletion of stratospheric ozone and the creation of the ozone hole over Antarctica (Molina & Rowland, 1974; Dhomse et al., 2019). Anthropogenic HVOCs such as carbon tetrachloride (CCl_4) and chlorofluorocarbons (CFCs) are inert and unable to breakdown in the troposphere. They are broken down through photolysis, and the released halogen atoms like chlorine catalytically destroy ozone molecules (Molina and Rowland, 1974; Carpenter et al., 2014). Due to the threat of these compounds to the ozone layer, policymakers developed the Montreal Protocol, a global agreement to ban production of ozone depleting compounds (Carpenter et al., 2014). CCl_4 and CFCs were part of the initial ban in 1996, and other compounds continue to be added such as certain hydrochlorofluorocarbons (HCFCs) and halons (Carpenter et al., 2014)

While anthropogenic HVOCs are well studied in the atmosphere, they are useful in oceanographic studies as well. Due to the inert nature of many anthropogenic HVOCs, such as CFCs, they can be used as powerful tracers that can determine water mass age and transport in the ocean (Bullister and Weiss, 1983; Fine, 2011; Orsi et al., 2002). The overall age of the water could be determined by comparing the concentration of CFCs in

the water at time of measuring to the supposed atmospheric concentration that water mass last was at the surface through Henry's Law. The ratio of two specific CFCs, CFC-11 and CFC-12 are commonly used. Since their ban, the ratio between the two compounds has remained steady. Therefore, sulfur hexafluoride (SF_6) was added the CFC-11/CFC-12 ratio to further determine water mass age.

Anthropogenic HVOCs are studied less in estuaries. Limited studies show elevated concentrations near wastewater outfalls of some anthropogenic HVOCs (Clark et al., 1995), with loss in the water assumed to be sea to air flux to the atmosphere (He et al., 2013). However, other removal mechanisms are rarely considered. CCl_4 and CFC-11 can adsorb to particulates and be sequestered to deeper waters in some fjords (Tanhua and Olsson, 2004). Once considered inert, CCl_4 is undersaturated in the surface ocean and presumed to undergo biological degradation (Butler et al., 2016). Limited research exists on the removal processes for chloroform ($CHCl_3$) and perchloroethylene (PCE) in estuaries, however loss of PCE has been modeled in Delaware River (Ambrose, 1987).

This study presents results of a year-long survey of anthropogenic HVOCs in Galveston Bay, TX following natural and anthropogenic forcing events. Galveston Bay is heavily influenced by the city of Houston, TX, and the Houston Ship Channel that is one of the busiest ports in the world. This provides a good location to study the fate and transport of anthropogenic HVOCs in estuarine settings. This setting also provides an opportunity to study and understand loss mechanisms outside of sea to air flux and their potential impacts on the water concentration throughout Galveston Bay and its freshwater endmembers

2. BACKGROUND

2.1. Carbon Tetrachloride

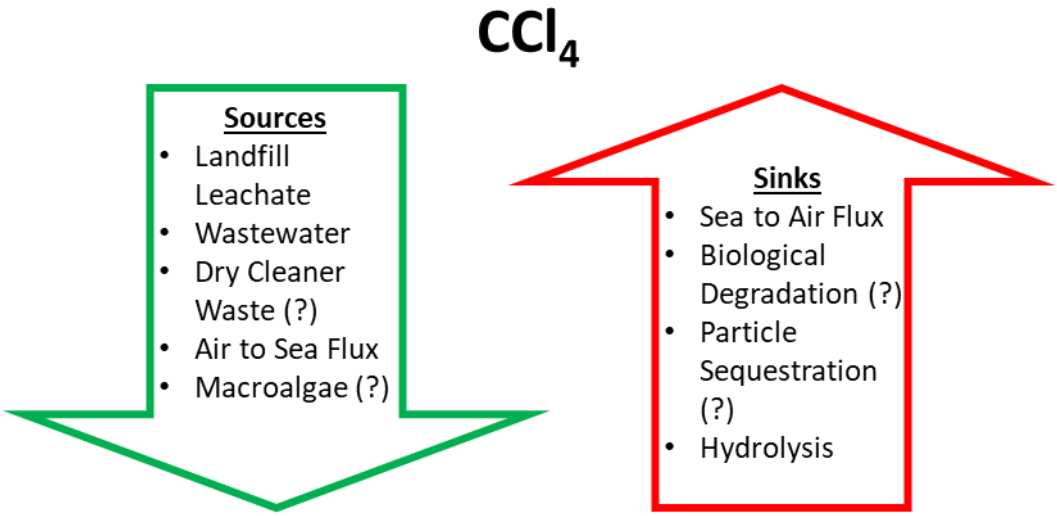

Figure 1: Sources and sinks of carbon tetrachloride (CCl_4) in estuaries. (?) denotes that the potential or significance is unknown

2.1.1. Sources

Industrialized regions of the southern United States, eastern China, and Europe have air concentrations higher than the global average for CCl_4 (Sherry et al., 2018). Measurements performed off the coast of China indicate emissions increasing over time, from 14 (9-19) Gg/year in 2006-2008 to 23.6 ± 7.4 Gg/year in 2011-2015 (Park et al., 2018; Vollmer et al., 2009). The location of the emissions remained constant throughout the two studies. The United States Environmental Protection Agency (USEPA) reports total emissions of 0.06 Gg/year in the United States. However, measurements of CCl_4 from air flasks and aircraft profiles indicate calculated emissions of 2.0-6.5 Gg/year,

accounting for 8% (3-22%) of total global emission (Hu et al., 2016). European emissions were an average of 2.2 ± 0.8 Gg/year from 2006-2014, accounting for 4.0% of the total global emissions (Graziosi et al., 2016), with Australian emissions currently measured at 165 ± 45 Mg/year (Fraser et al., 2014). Emissions in the United States and Europe are at chemical production and industrial sites (Graziosi et al., 2016; Hu et al., 2016). Australia has no significant industrial influence as CCl_4 has not been imported or used as a feedstock since the 1980s (Fraser et al., 2014).

While most emissions are direct to the atmosphere, there are also direct sources to water bodies. Chlor-alkali chemical plants can release CCl_4 by fugitive emission or wastewater (Amaral et al., 1996; Fraser et al., 2014; Graziosi et al., 2016; Hu et al., 2016; Sherry et al., 2018). A total of 80% of the global chlor-alkali production is in the regions of East Asia (48%), North America (19%), and Western Europe (16%) (Brinkmann et al., 2014). Due to the many uses of CCl_4, contaminated items not disposed of correctly in historic landfills and nuclear reservation sites could potentially leak CCl_4 into groundwater, soil, and the atmosphere (Carnes & Watson, 1989; Sherry et al., 2018). Estuaries affected by anthropogenic forcing, such as Galveston Bay, could see increased halocarbon concentrations from these wastewater sources. In Germany, the Elbe estuary, affected by effluent water from industrial areas, display supersaturations over 200% near industrial centers (Dyrssen et al., 1990). Higher concentrations are exhibited at low tide for carbon tetrachloride, suggesting that the freshwater inputs are a source over the tidal ocean. Coastal salt marshes tend to act as an overall sink of CCl4. However, the flux of carbon tetrachloride varies from location to location, with

occasional high fluxes to the atmosphere (Wang et al., 2007). In areas containing macroalgae, carbon tetrachloride emissions tend to be higher, suggesting the potential for a natural source and higher water concentrations (Rhew et al., 2008).

2.1.2. Sinks

CCl_4 degrades slowly in the atmosphere, soil, and ocean. The only known removal process in the atmosphere is photolysis in the stratosphere (Butler et al., 2016; Molina & Rowland, 1974; Rontu Carlon et al., 2010). The magnitude of the atmospheric lifetime depends on interannual meteorological variability, giving a partial atmospheric lifetime in models of 39.5 to 46 years (Chipperfield et al., 2016). The degradation of CCl_4 in soils varies with the composition and conditions of each soil. In anaerobic settings, abiotic transformation by iron-containing components in the soil such as FeS, FeS_2, magnetite, and goethite can reduce CCl_4 to chloroform (Amonette et al., 2000; Shao & Butler, 2009). In aerobic settings, the upper 15 cm of soil is the most active removal zone suggesting biological degradation and organic matter content in the soil play a significant role in dechlorination (Collins & Picardal, 1999; Happell & Wallace, 1998; Mendoza et al., 2011; Temme et al., 2019).

The removal processes of CCl_4 in the ocean remain relatively unknown. Currently, only hydrolysis, a process that takes thousands of years, and sequestering into deeper waters are the quantified removal processes (Azetsu-Scott et al., 2005; Mabey & Mill, 1978; Wallace et al., 1994; Yvon-Lewis & Butler, 2002). However, these processes alone do not account for the nearly global undersaturation of the CCl_4 in the surface ocean. A potential removal process from the surface and intermediate waters is CCl_4 adsorbing to

particulate matter then being sequestered in deep water (Tanhua & Olsson, 2005). This process can occur in semi-enclosed basins such as Framvaren Fjord and only accounts for 1-5% of deep-water accumulation. Adherence to particulate organic matter is hypothesized to be a source of CCl_4 to deeper waters (Min et al., 2010) and may play an important role in sequestering this compound to the sediments of estuaries.

2.1.3. Biological Degradation

Bacterial degradation of CCl_4 in other mediums can inform what may be the processes contributing to removal in the ocean. The reduction of CCl_4 occurs in anaerobic conditions as the lack of oxygen allows CCl_4 to behave as an electron acceptor. CCl_4 degrades in methanogenic, iron-reducing, sulfate-reducing, and fermenting conditions in the presence of electron acceptors suitable for one or all above conditions (Boopathy, 2002; Egli et al., 1988, 1990; Jappe et al., 1998; Koenig et al., 2012; Krone et al., 1991; Picardal et al., 1993). Degradation products observed for these experiments include chloroform, dichloromethane, methyl chloride, carbon dioxide, carbon monoxide, acetate, pyruvate, and cell material (Boopathy, 2002; Egli et al., 1988, 1990; Jappe et al., 1998; Koenig et al., 2012; Krone et al., 1991; Picardal et al., 1993). Organohalide respiring bacteria are likely responsible for this in anaerobic settings as they contain the membrane-bound enzyme reductive dehalogenase, which can break down halogenated compounds (Jugder et al., 2015, 2016). Non-enzymatic pathways through the reduction of cobalamin cofactors, organic matter, and humic acids, which subsequently attack and reduce CCl_4, are possible as well (Collins & Picardal, 1999; Egli et al., 1990; Penny et al., 2010; Zou et al., 2000).

The observed undersaturation of CCl_4 in the surface waters point towards an aerobic degradation pathway even though CCl_4 is a fully oxidized compound. However, the enzyme or process for reduction or substitution of CCl_4 is unclear and hard to pin down. Some oxidizing bacteria can transform CCl_4 through hydrogenolysis faster than anaerobic bacteria (Castro, 1993). Other bacteria show an ability to readily produce haloalkane, haloacid, and reductive dehalogenases regardless of previous exposure to chlorinated compounds (Temme et al., 2019). Haloalkane and haloacid enzymes capable of optimally degrading CCl_4 at a pH of 8.0 (Olaniran et al., 2004; Olaniran et al., 2002). Other aerobic pathways observed in some bacteria create two free radical species, a trichloromethyl radical and elemental chlorine, due to the strength of the carbon-chloride bonds that cause CCl_4's toxic nature (Penny et al., 2010). There is potential that a bulk toxic path over a specific biological degradation path could be the root cause of the degradation of this compound in surface waters.

2.2. CFC-11

2.2.1. Sources

Chlorofluorocarbons (CFCs) are anthropogenic compounds that were banned along with CCl_4 by the Montreal Protocol in 1996 due to their ozone depletion potential. CFC-11 was produced through fluorination of CCl_4 and saw use predominantly for refrigeration, air conditioning, a propellant in aerosol cans, and a foam blower for insulation foam (Khalil and Rasmussen, 1993). Antarctic firn data show that any natural source has minimal contribution to the atmospheric burden (Butler et al., 1999). The only known potential natural source of CFC-11 is volcanic eruptions containing

hydrogen fluoride, but studies show ambient air with higher concentrations of CFC-11 compared to volcanic vents in multiple sites (Isidorov, 1990). Older homes may still contain insulation blown with CFC-11 propellant, representing a bank of the chemical still present today. However, this bank decreases and contributes less each year to the atmospheric burden (Montzka et al. 2018). However, increased emissions of CFC-11 have been observed in China in similar regions as CCl_4 (Montzka et al., 2018; Rigby et al., 2019). With a derived global emission determined to be 68.0 ± 6.4 Gg yr^{-1}, a potential delay in the Antarctic ozone hole recovery is predicted (Montzka et al., 2018; Dhomse et al., 2019).

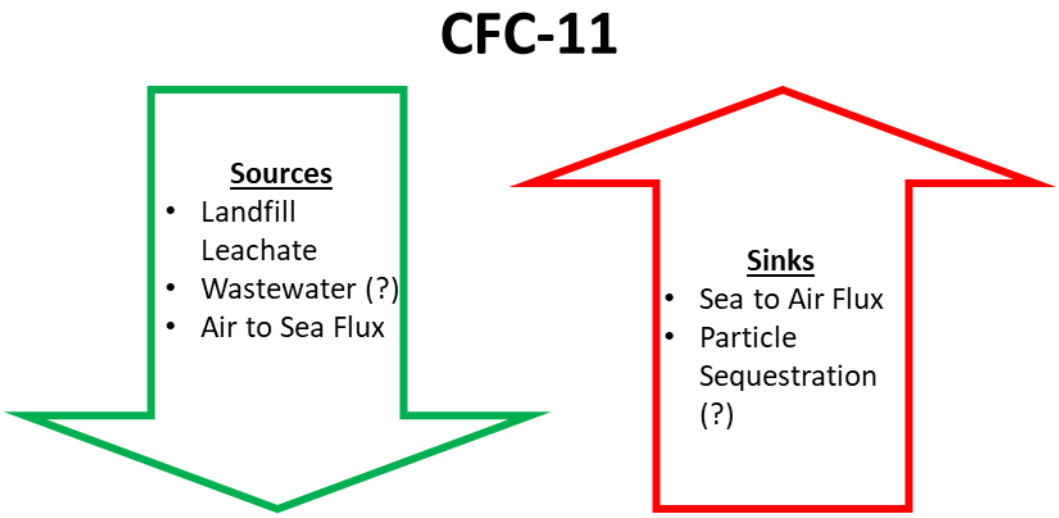

Figure 2: Sources and sinks of CFC-11 in estuaries. (?) denotes that the potential or significance is unknown.

Due to its inert nature, CFC-11 in tandem with CFC-12 is a tracer of water mass age, formation, and transport (Bullister & Weiss, 1983; Fine, 2011; Min et al., 2002; Orsi et al., 2002). CFCs mix conservatively throughout the water column. The ratio

between the two compounds in water be used to estimate when the water mass was last at the surface. However, in turbulent, shallow systems such as estuaries, continual air-sea exchange limits the use of CFCs in this way. Therefore, CFC-11 concentrations in estuaries above equilibrium is either due to physical injection through breaking waves or direct anthropogenic input. Overall concentrations of CFC-11 are higher throughout some estuaries, with the highest concentrations found near wastewater outfalls (Clark et al., 1995). Therefore, CFC-11 can be and has been used as a tracer of wastewater, but the exact point sources are unknown.

2.3. Chloroform ($CHCl_3$)

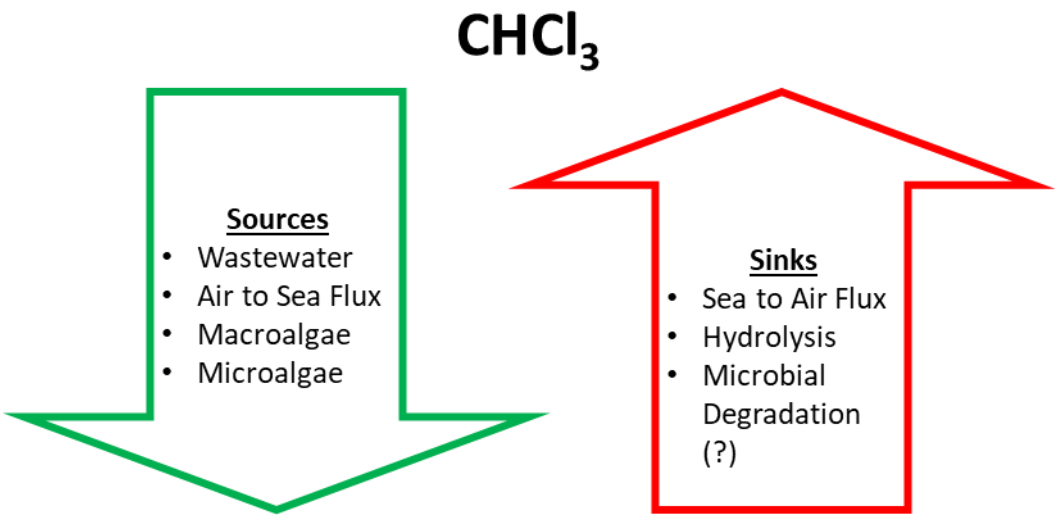

Figure 3: Sources and sinks of chloroform ($CHCl_3$) in estuaries. (?) denotes that the potential is unknown.

2.3.1. Sources

Unlike the other chlorinated compounds discussed above, natural sources of $CHCl_3$ into the environment dwarf any estimated anthropogenic input. Roughly 90% of

the source of chloroform into the environment is through natural means (McCulloch 2003). Oceanic emissions to the atmosphere are estimated to be 360 ± 90 Gg yr^{-1} with 270 Gg yr^{-1} emitted by the coastal ocean alone (Khalil and Rasmussen, 1999; Nightingale et al., 1995; McCulloch 2003). In coastal ocean settings, $CHCl_3$, along with other trihalomethanes (THMs), are produced by various macroalgae species as an antimicrobial agent or grazing deterrent (Nightingale et al., 1995). The enzyme necessary to produce $CHCl_3$ is the chloroperoxidase enzyme (CPO), found in various algae species such as diatoms and algae (Hong et al., 2008; Nightingale et al., 1995). Chloroform and other THMs are ubiquitous in potable and wastewater treated by chlorine and ozone (McCulloch, 2003), therefore populated coastal areas may impact the production of $CHCl_3$ through increased nutrient and wastewater loading of the area.

Soil processes emit 220 ± 100 Gg yr^{-1} of $CHCl_3$ to the environment primarily through biological processes (Keene et al. 1999). Significant emissions of THMs occur in unpopulated regions, coastal peatland, and rainforests (McCulloch 2003; Cox et al., 2001; Ryall et al., 2001). As the Arctic climate warms, the release of $CHCl_3$ may increase due to warmed tundra, peatland, and encroached coniferous forests (Rhew et al., 2008; Johnsen et al., 2016). Studies show that CPO sourced through fungal species create the hypochlorous acid in the presence of hydrogen peroxide and hydrogen and chlorine ions (McCulloch 2003). The hypochlorous acid then reacts with humic material in the soil to create chloroform and other THMs. Other minor terrestrial sources, such as volcanic events, provide little to no impact on the flux of $CHCl_3$ globally (McCulloch 2003).

The total anthropogenic emission of $CHCl_3$ is less than 70 Gg yr^{-1} from various industrial processes (McCulloch 2003). Paper and pulp manufacturing produce chloroform through delignification and bleaching of paper that contain chlorine, with estimates of global emission at 34 Gg yr^{-1} (Aucott et al., 1999). Cooling water, drawn from rivers and estuaries that contain humic material, treated with chlorine to disinfect the water pipes can contain increased chloroform. Coupled with water treatment plants that use chlorine as a disinfectant, emission of 9 ± 6 Gg yr^{-1} comes from these combined pathways (Aucott et al., 1999). Another potential source is the emission from chlorinated swimming pools, as $CHCl_3$ concentration in pools can range from 23,000 – 450,000 ng m^{-3} (McCulloch 2003). The potential impact of this is more likely to affect air concentration locally rather than globally. Production of $CHCl_3$ as a feedstock for other halogenated compounds and as a solvent lead to an estimated emission of 11 Gg yr^{-1} (Aucott et al., 1999). Most of the anthropogenic source of $CHCl_3$ is the Northern Hemisphere, as most of the human population and land surface area is in this hemisphere. A recent study found increases in $CHCl_3$ emissions from 2010-2015 in China by 49 (41-59) Gg yr^{-1}, explaining the recent increase of global emissions of $CHCl_3$ (Fang et al. 2019).

2.3.2. Sinks

Removal of $CHCl_3$ occurs through various processes in the atmospheric, aquatic, and terrestrial environments. The primary degradation process is oxidation by the hydroxyl radical in the atmosphere, which removes 600 Gg yr^{-1} (Khalil & Rasmussen, 1999). $CHCl_3$ is a very short-lived substance (< 0.5 yrs) and the second most crucial

chlorine-loading chemical to the troposphere and stratosphere behind methyl chloride (Rhew et al., 2008). Soil removal processes can occur aerobically through microbes that have the methane monooxygenase enzyme, producing carbon dioxide as a byproduct (McCulloch 2003). In the ocean, hydrolysis is the only known removal pathway with a half-life of 1000 years. In anoxic waters, redox reactions degrade chloroform (Tanhua et al. 1996). Redox reactions could play a role in removal in anoxic groundwater even though $CHCl_3$ concentrations can reach upwards of 500 ng L^{-1} and are increasing in some aquifers (McCulloch 2003).

2.4. PCE

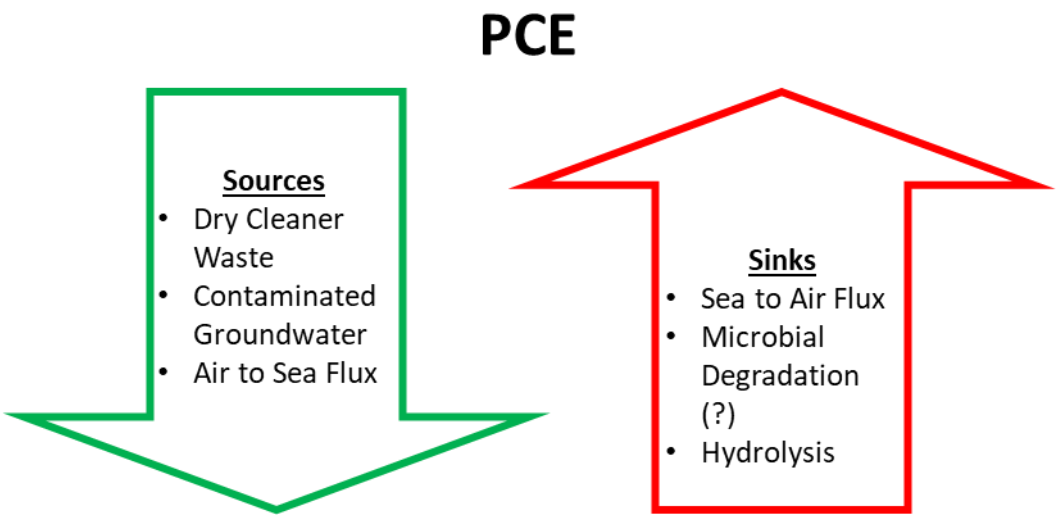

Figure 4: Sources and sinks of perchloroethylene (PCE) in estuaries. (?) denotes that the potential is unknown.

2.4.1. Sources

Perchloroethylene (PCE) is used as a replacement for CCl_4 for dry-cleaning, metal degreasing, oil refining, and feedstock for some hydrochlorofluorocarbons

(HCFCs) and hydrofluorocarbons (HFCs). A smaller portion of PCE is used for various commercial and consumer products, such as adhesives, lubricants, and sealants. Due to its high volatility, PCE predominantly evaporates into the atmosphere before polluting water or soil. However, PCE spilled onto soil can leach into the groundwater below. PCE is also denser than water, and as a nonaqueous liquid can sink below the water table and remain a persistent pollutant source to groundwater (Tsai et al., 2009). Rivers and estuaries fed by contaminated groundwater sources can have elevated concentrations of PCE (Wittlingerova et al., 2016). No global ban exists for PCE, but the USEPA set a maximum contaminant level of 5 μg L^{-1} (U.S. EPA, 2009).

Recent studies found a potential natural source of PCE to the estuarine and coastal systems. Cultures of diatoms *Phaeodactylum tricornutum* and *Chaetoceros neogracilis* and chlorophyte species *Dunaliella tertiolecta* show elevated headspace concentrations of PCE (Colomb et al. 2008). The formation of PCE in natural settings is currently unknown. However, haloperoxidase enzymes may chlorinate ethene and eventually form PCE through addition and reduction reactions (Abrahamsson et al., 1995; Ballschmiter, 2003). Anthropogenic impacts are more likely to affect coastal areas impacted by urban or industrial activities, even with the capability of natural sources.

2.4.2. Sinks

Due to the volatility of PCE, most of the compound enters the atmosphere. The primary removal process is the reaction with hydroxyl radicals, with an estimated lifetime for this compound of 0.43 years (WMO, 1991). In water, the only known abiotic degradation pathway is hydrolysis, leading to an oceanic lifetime of over 400,000 years

(Yvon-Lewis & Butler, 2002). In oxygenated waters, incubation studies found that combinations of conditions or bacteria were unable to degrade PCE, including sewage effluent or groundwater infiltration to surface water (Bouwer et al., 1981; Fogel et al., 1986; Schwarzenbach et al., 1983; Vannelli et al. 1990). However, a recent study determined that phototrophic bacteria in the presence of organic carbon can rapidly degrade PCE in aerobic settings (Mun & Kirienko, 2011). In anaerobic settings, PCE degradation mainly occurs through reductive dechlorination with trichloroethene (TCE), dichloroethane, ethene, and ethane as the main products. Methanogenic and sulfate-reducing bacteria can degrade PCE through cometabolic processes, but methanogenic bacteria degrade it at a faster rate (Suflita et al., 1988).

3. SITE DESCRIPTION: GALVESTON BAY

3.1. Background

Galveston Bay is a large microtidal estuary (1360 km^2) along the Texas coast and is home to the city and port of Houston, the fourth busiest seaport in the world with over 7800 vessel calls per year. Overall, the bay itself is shallow, with an average depth of 2.4 m, except for the Houston Ship Channel, a dredged 200 m wide channel throughout Galveston Bay leading to the Gulf of Mexico that is on average 15 m deep. Galveston Bay is classified as a coastal lagoon with a barrier island and four major embayments (Galveston, Trinity, East, and West Bays) separated by either anthropogenic or natural dikes or reefs (Figure 5). Due to this separation or lack thereof, residence times within Galveston Bay vary (Rayson et al., 2015). The Redfish Reef, a natural oyster reef, limits water exchange between Upper Galveston Bay and Trinity Bay with Lower Galveston Bay outside the Houston Ship Channel. East Bay is characterized mostly by the natural oyster reefs that inhabit the shallow waters of the area and limit saltwater intrusion. West Bay's natural sheltered region is a feeding ground for turtles and other marine animals (Shaver et al., 2017). Most of the tidal influence into the bay is from the Bolivar Roads entrance into the Gulf of Mexico near Galveston Island (80%), with West Bay and East Bay influenced by tidal exchange with the San Luis Pass and Rollover Pass, respectively (Orlando, 1993).

Trinity Bay is fed by Trinity River, which provides roughly 75% of the freshwater input into Galveston Bay. Despite how shallow the bay is, Trinity Bay is the only area

outside of the Houston Ship Channel that exhibits stratification within the water column (Orlando, 1993). Stratification mainly occurs during times of high flow from Trinity River, where freshwater input to the bay has more of an effect on the salinity than the tidal influences of the Gulf of Mexico. Overall, the Trinity River freshwater input into Trinity Bay, and by extension, all of Galveston Bay, control the salinity structure (Orlando, 1993). Upper Galveston Bay receives freshwater input from Buffalo Bayou (6%) and the San Jacinto River (8%). The two freshwater inputs converge into the Lower San Jacinto region before entering the bay and have little effect on the overall salinity structure of the Bay. San Jacinto River runs alongside the City of Houston, while

Buffalo Bayou runs through downtown Houston and houses the freshwater endpoint of the Houston Ship Channel at the Turning Basin.

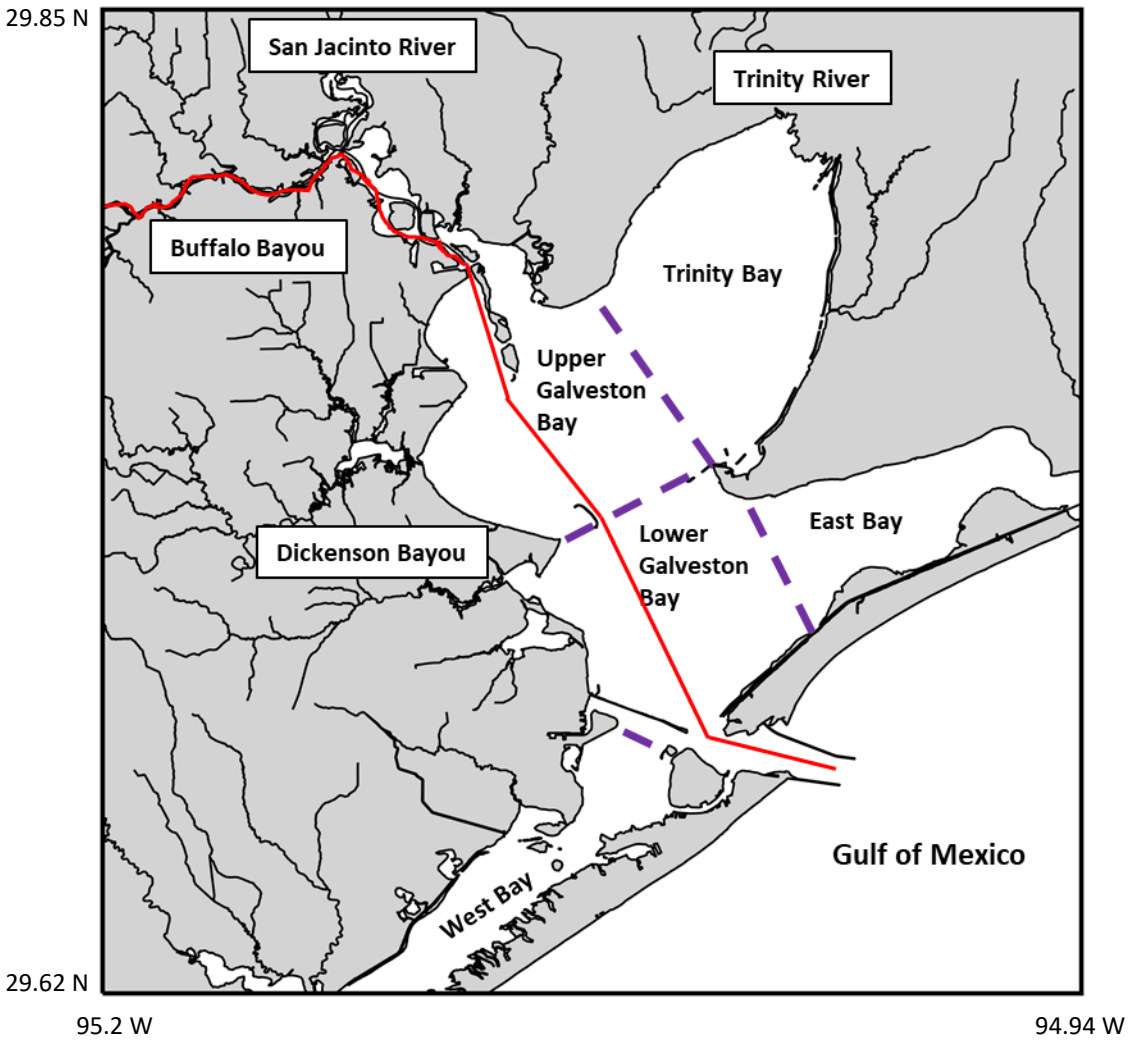

Figure 5: Map of Galveston Bay with the sub-bays sectioned off by purple dashed lines. The solid red line marks the path of the Houston Ship Channel. Sampled freshwater inputs into Galveston Bay are labeled.

3.2. Potential Anthropogenic Influences on the Bay

Due to the proximity to the megacity of Houston, Galveston Bay experiences influence through industrial and domestic wastewater outfalls, leaking petroleum tanks,

dry cleaner waste sites, and municipal solid waste sites in the region (Figure 6). Many Texas Commission of Environmental Quality (TCEQ) superfund sites contain chemicals such as PCBs and dioxins. Chemical plants and storage facilities are dominant along the Buffalo Bayou and Dickinson Bayou regions. Industrial cleaning facilities are present along Dickinson Bayou as well. While industrial activity dominates the western coast of Galveston Bay, the eastern coast is predominantly farmland and wildlife refuges. Trinity River flows through the Dallas-Fort Worth area and agricultural land, before flowing into Trinity Bay. East Bay, due to the wildlife refuges, most likely sees little anthropogenic input. However, the Gulf Intracoastal Waterway, a controlled 3.7 m deep channel that runs along all Gulf Coast states, provides ship traffic, mainly barge transport, through East Bay and West Bay.

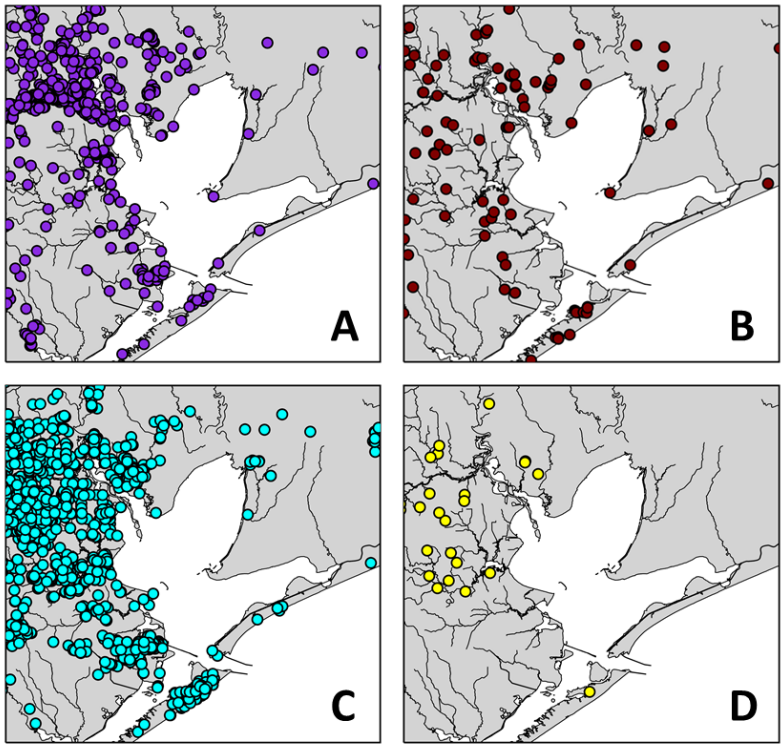

Figure 6: Location of wastewater outfalls (A), municipal solid waste sites (B), leaking petroleum storage tanks (C), and dry cleaner waste sites (D) around Galveston Bay. Municipal solid waste sites listed are closed due to lack of operation permit. Location of sites obtained from TCEQ.

3.3. Buffalo Bayou and the Houston Ship Channel

The Houston Ship Channel (HSC) was completed in 1914 and is 83.7 km long, 160 m wide, and on average 13.7 m deep. Currently, the impacts and benefits of the HSC generate over $800 billion dollars in revenue with over 7800 vessel calls per year. The Port of Houston itself due to the HSC is the leading United States port for exports, foreign commerce, and petrochemical manufacturing. The HSC extends into 25 km of Buffalo Bayou, from the mouth of the bayou at the Lower San Jacinto region to the Turning Basin. In the Buffalo Bayou section of the HSC, over 200 private and public

facilities and the largest concentration of wastewater outfalls and leaking petroleum storage tanks in the region in the Galveston Bay region (Figure 6). Persistent organic pollutants, such as dioxins and polychlorinated biphenyls (PCBs), are ubiquitous in water, soil, and biota of this region and make the HSC in Buffalo Bayou one the most contaminated industrial areas in the world (Lakshmanan et al., 2010)

Despite the creation of the HSC over 100 years ago, few studies or analyses are done consistently to understand the temperature and salinity profiles within the channel itself. Models determine that the HSC is stratified, with the stratification less pronounced to nonexistent in Lower Galveston Bay (Bobb et al., 1973; Rayson et al., 2015). The stratification depth responds to the discharge rate of the Trinity River in the Lower Galveston Bay region (Rayson et al., 2015). In the Buffalo Bayou and Lower San Jacinto regions of the HSC, modeled data shows a potential increase of strengthening of the halocline in the region (Bobb et al., 1973). Overall, above Redfish Reef into Upper Galveston Bay, the surface layer extends to two to four meters of depth depending on the freshwater flow rate and tidal currents (Rayson et al., 2015; Schmalz, 2000).

3.4. Natural and Anthropogenic Events

Due to its location near Houston and the Gulf of Mexico, natural and anthropogenic events on a wide scale of severity affect Galveston Bay. Since 2004, there has been an average of 226 oil spills reported per year, with most spills less than five gallons (Galveston Bay Report Card, 2020). However, large spills can occur such as in September 2016 where a shipping vessel released 88,000 gallons of diesel fuel into the Houston Shipping Channel. Significant widespread drought in Texas from 2011-2012

increased the salinity of Galveston Bay. Tropical storms and hurricanes have devastated the region and Galveston Bay. Of recent note, Tropical Storm Allison caused an accumulated rainfall of over 35" in Houston in 2001. Hurricane Ike in 2008 made landfall as a Category 2 Hurricane and was known for its devasting storm surge and winds, heavily damaging the island of Galveston. Hurricane Harvey in 2017 took an unusual track, making landfall initially in Rockport, Texas as a Category 4 Hurricane before returning to the Gulf of Mexico, where it stalled before making landfall in Cameron, Louisiana. Houston received over 60" of rain from Harvey, and over 1150 km^2 of Harris County flooded. Harvey also caused over 50 tornadoes along its path. Galveston Bay remained fresh for over a month before tidal mixing began to increase the salinity. Therefore, defining "normal" conditions of water composition in Galveston Bay is a challenging endeavor. The minimum flushing time of 20 days for Galveston Bay determined from a model of Lagrangian residence time (Rayson et al. 2016) leads to prolonged effects from any forcing events.

During the sampling period of this study, two events occurred that impacted Galveston Bay. On March 17, 2019, a chemical fire began at the Intercontinental Terminals Company (ITC) in Deer Park, TX, after 9000 gallons of a Naptha-Butane mixture leaked from a storage tank. A stay-in-place order was issued during this time due to the high levels of benzene released into the air. The fire ended the morning of March 20th, destroying eight storage tanks in the ITC storage farm. On March 22nd, a containment wall surrounding the storage tank farm collapsed, releasing liquid

containing firefighting foam and unknown chemicals from destroyed storage tanks not consumed by the fire into Tucker Bayou, which feeds into Buffalo Bayou.

On September 17th, 2019, Tropical Storm Imelda made landfall at Freeport, TX, 80 km south of Houston. Imelda developed from a tropical depression, to a tropical storm, to making landfall in an hour and a half. Labeled the fifth wettest tropical cyclone in the contiguous United States, anywhere from 30-43" of rain fell in the San Jacinto River and Trinity River watersheds, with roughly 16" of rain falling directly onto Galveston Bay itself. While not as devastating a storm as Hurricane Harvey, significant flooding of Southeast Texas occurred, and there is potential for a flushing event to have occurred in the Bay.

4. OBJECTIVES AND HYPOTHESES

4.1. Objectives

The primary objective of this study is to obtain baseline concentrations for a suite of HVOCs and examine the spatial and temporal variations in the surface water and atmosphere of Galveston Bay, TX. Due to the anthropogenic inputs and origins of the investigated compounds, the impact of flowrate from the Lower San Jacinto region and the Houston Ship Channel into Galveston Bay should affect the concentrations of the compounds and be the primary source. Throughout the sampling period in 2019, the events of the ITC fire in Deer Park, TX, and Tropical Storm Imelda led to determining the impacts of natural and anthropogenic forcing on the concentrations of HVOCs. A model of the net change in concentration comparing production and loss is employed to determine whether known loss and input parameters are enough to understand this system.

4.2. Hypotheses

1. Higher concentrations of all HVOCs will be measured near areas of high anthropogenic activity during the entire sampling period.
2. Flux to the atmosphere will not be large enough to account for the loss of each compound from the surface waters within the San Jacinto/Houston Ship Channel region.

3. No discernable increase or decrease in concentration for any of the specified HVOCs is expected following the ITC fire in Deer Park, TX, as these compounds should not be contained at ITC or used in the firefighting process.

4. Tropical Storm Imelda flushed Galveston Bay, leading to lower than average concentrations and saturation anomalies for all compounds.

5. METHODS

5.1. Field and Analytical Methods

Galveston Bay seawater samples were collected using 100 mL ground glass syringes from a 5L Niskin collection bottle aboard the R/V Trident at multiple stations (Figure 7). Surface samples were prioritized. However, due to equipment complications, a mix of surface and bottom samples is used to determine spatial variations in the bay. Samples are immediately filtered through 0.2-micron Mediakap filters and injected through PEEK tubing into a 70 mL calibrated glass bulb stored in a refrigeration unit kept at 6 °C. A total of 15 samples are collected on each cruise, with a priority towards collecting surface samples. Bottom depths of 1.22 m from max depth are taken at stations exhibiting a salinity gradient. Duplicates are also collected on each cruise. Air samples are collected at three stations during each cruise to determine each HVOC's average air concentration for the Galveston Bay area. Samples for dissolved oxygen (DO), dissolved organic matter (DOM), colored dissolved organic matter (CDOM), nutrients, pH, dissolved inorganic carbon (DIC), alkalinity, and per- and polyfluorinated alkyl substances (PFAS) were collected and analyzed by other researchers aboard.

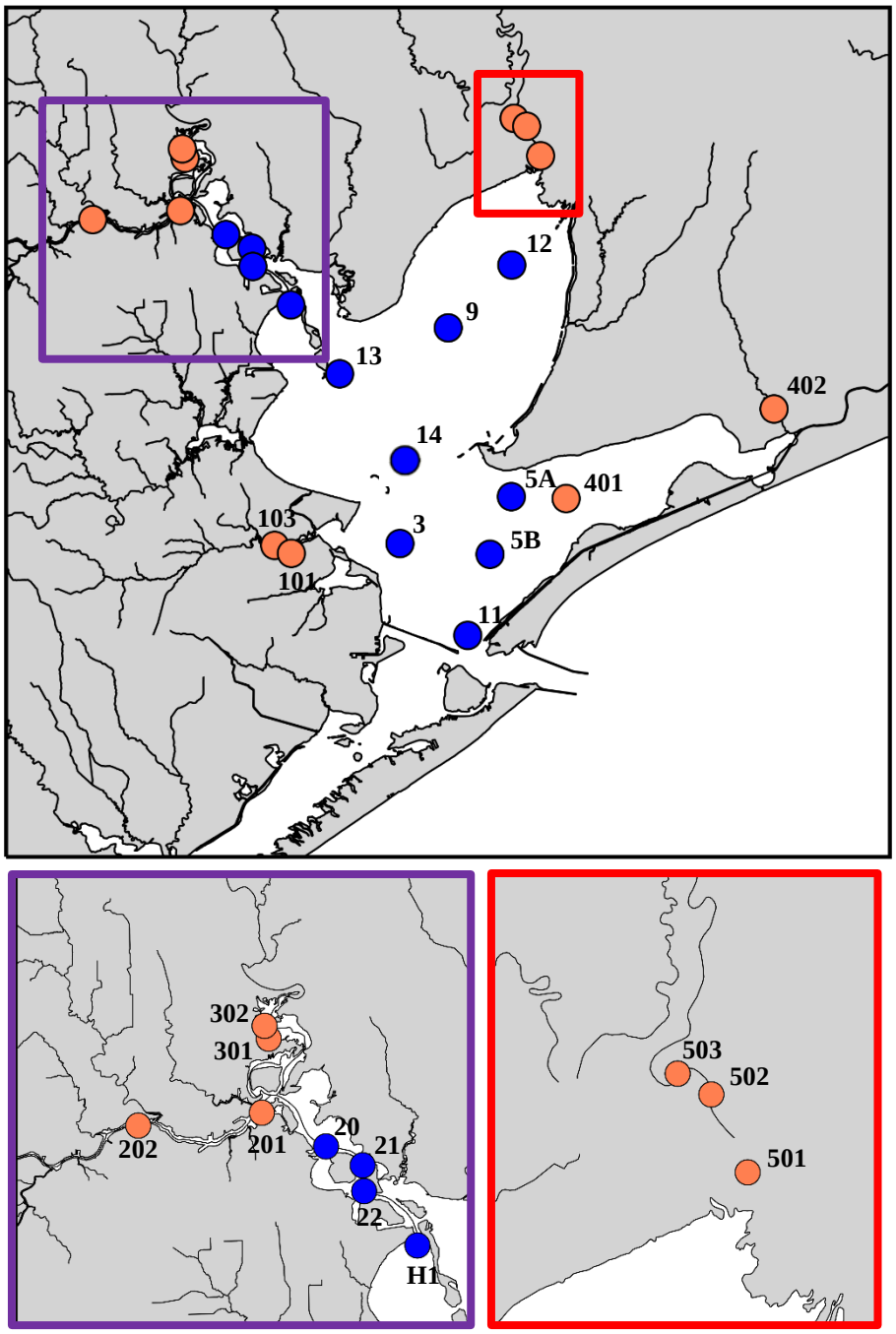

Figure 7: Map of stations sampled in Galveston Bay and the freshwater endmembers. Stations marked with a blue circle were sampled in all four cruises if possible, while the orange stations were sampled during the freshwater endmember cruises on June 15-16, 2019 only. The purple box is the Lower San Jacinto, Buffalo Bayou, and San Jacinto River stations sampled. The red box is the Trinity River stations sampled.

Table 1: Stations and depths sampled for HVOCs for each cruise date. S is the surface depth, while B is the bottom depth. x indicates sampling, blank means no sampling was performed. Station locations are shown in Figure 7.

Station	Cruise Date									
	March		June (Endmembers)		June (Galveston Bay)		September		November	
	S	B	S	B	S	B	S	B	S	B
1	x				x					
3	x	x			x			x	x	x
5A					x		x		x	
5B	x				x			x		
9	x	x			x			x	x	
11	x				x	x	x	x	x	x
12	x				x			x	x	
13	x	x			x	x		x	x	x
14	x	x					x		x	x
20	x				x		x		x	
21									x	
22	x						x		x	
H1	x						x		x	
101, 103			x							
201, 202			x							
301, 302			x							
401, 402			x							
501, 502, 503			x							

Each bulb is flushed and purged separately with ultra-high purity nitrogen gas at 135 mL/min at 40 °C. The sample is then subsequently dried by two in-line Nafion dryers. The analytes are then preconcentrated onto the first of two cryotraps packed with Unibeads 1S (80/100 mesh) kept at -80 °C (1.5 mm ID). The analytes are then refocused onto the second steel trap (0.75 mm ID) before injection into an Agilent Model 7890A Gas Chromatograph containing a PoraBOND Q PLOT pre-column (5 m, 0.32 mm ID, 5

um film thickness) and main column (20 m, 0.32 mm ID, 5 um film thickness) with helium carrier gas for separation (Figure 8). The column temperature is ramped (40 °C initial and held for one minute, followed by a 22.9 °C/min ramp until 200 °C, which is held for the duration of the run) to achieve separation of halocarbons, similar to the Medusa system used by AGAGE (Miller et al., 2008). Compounds in the sample are detected with a quadrupole mass spectrometer (Agilent 5975) using selective ion mode (SIM) for increased sensitivity. Each specific SIM window contains a maximum of 9 ions of every monitored compound (Table 2).

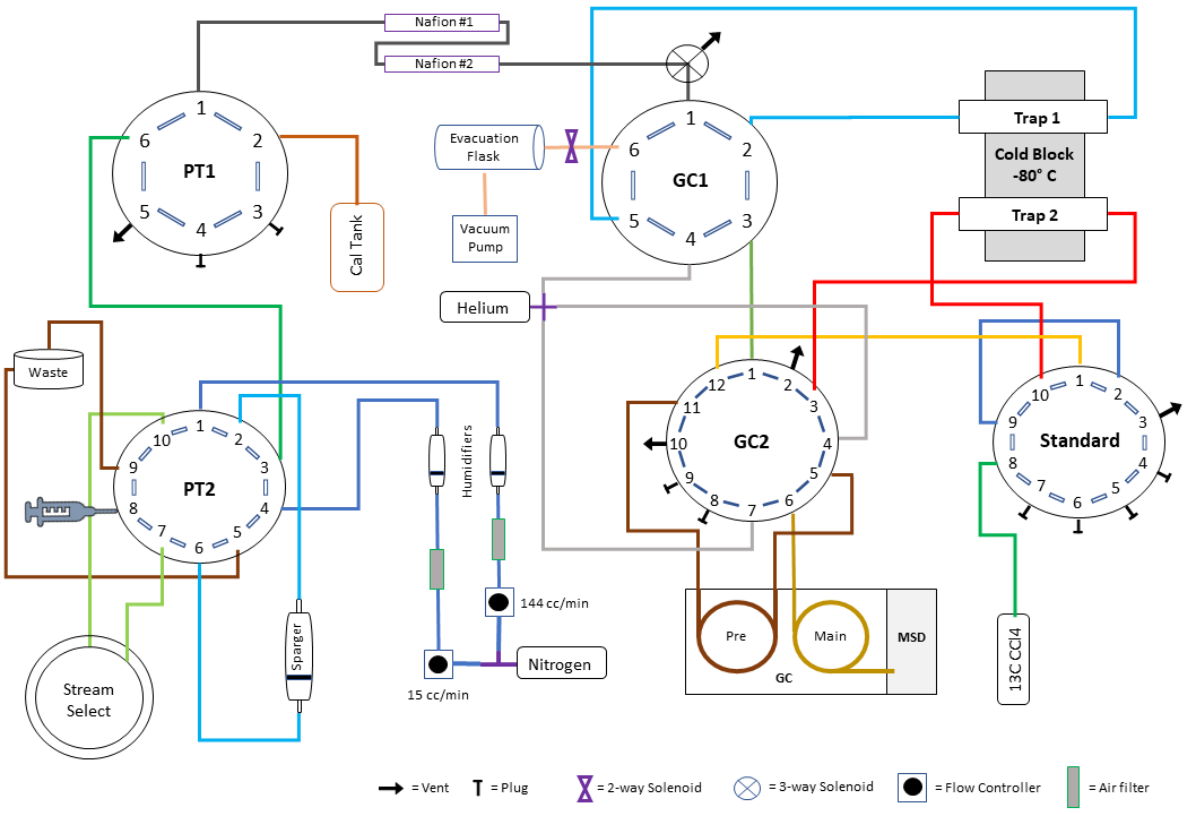

Figure 8: Schematic of flow for Purge and Trap GC/MS. The Stream Select symbolizes the refrigeration unit containing 16 air-tight bulbs and a 16-position multi-position stream select valve. Valves PT1 and PT2 control the flow and processes for purging water samples, while valves GC1 and GC2 control focusing and transfer of sample gas into the GC/MS. The Standard valve has a 1 mL loop that is flushed with ^{13}C CCl_4 until moved in-line to transfer into GC/MS. This valve is not used for this experiment.

Table 2: Compounds analyzed during sample analysis. Ions in bold are the quantifying ions, others are identifying ions. Precision for each HVOC is the coefficient of variation determined from calibration of the air tank standard

Compound	Retention Time (min)	Ions	Precision
CFC-11	5.88	101, **103**, 105	4.4%
$CHCl_3$	7.07	**83,** 85, 87	6.4%
CCl_4	7.90	82, 84, 97, **117**	4.4%
PCE	9.47	129, 131, 164, **166**	8.8%

5.2. Method for Calibrating Air Tank Standard

A method for determining the HVOC concentration in an air tank was developed to obtain the concentration of water samples using the Purge and Trap GC/MS technique. A whole air calibrated air tank standard from the National Oceanic and Atmospheric Administration (NOAA) or the Scripps Institute of Oceanography (SIO) is used to determine the concentration of HVOCs in water samples with a Purge and Trap GC/MS (Yvon-Lewis et al., 2002). In a dark room, 120 mL vials and two glass beads were rinsed with Ultra High Purity Water (UHPW) (Sigma-Aldrich) and allowed time to dry. The glass beads were placed in the vials, then filled slowly with UHPW until a meniscus formed. Pouring water slowly and against the glass limited the chance to inject atmospheric air into the water.

An ampoule of 1 mL halocarbon primary standard (Absolute Standard) containing twenty-two different compounds at 200 nmol/mL, kept at -20 degrees Celsius, was removed from cold storage. The ampoule was cracked open, and a 1 mL syringe was rinsed three times by filling with 0.1 mL of the primary standard to rinse the walls of the syringe and remove any air bubbles. 0.3 mL of the primary standard was injected into the vial to create a secondary standard at an angle, then quickly capped and sealed with a Teflon cap on the vial. This method should introduce no air bubbles, and therefore no consideration of Henry's Law partitioning of gases should be necessary. The cap was covered with aluminum tape, and then the secondary standard was covered with aluminum foil to remove the potential of light hitting the sample. The vial was then

placed in an orbital shaker at 200 rpm for a minimum of two hours to mix the sample thoroughly. Secondary standards allowed to mix for two hours or twelve hours showed no discernable difference in concentration.

Four 150 mL ground glass syringes were rinsed three times then filled with two glass beads and UHPW to create the final tertiary standard. One syringe was selected at random and wrapped with an elastic band to act as the water blank. In a dark room, a 1 μL syringe was used to extract the secondary standard from the vial to create the tertiary standard. The 1 μL syringe was then placed through the Luer-lock tip and injected into the ground glass syringe. This step was repeated twice more to create the other tertiary standards. Elastic bands were placed around the ground glass syringe's plunger and tip to increase pressure within the tertiary standard to contain the halogenated compounds. Each tertiary standard syringe was then shaken vigorously for two minutes, then placed in a chilled unit kept at 6 C. The tertiary standards were then removed and shaken two more times after ten minutes to have a thoroughly mixed and equilibrated standard. Tertiary standards and the water blank were then run through the standard Purge and Trap GC/MS protocol against the air tank to be calibrated. Precision for measurement of HVOCs was determined during calibration and listed in Table 2.

6. RESULTS AND DISCUSSION

6.1. Water Quality Parameters and Freshwater Flow Rates

The temperature was consistent throughout the bay and end members, with higher temperatures occurring in the freshwater endmembers in June (Figure 9) Temporal variations in temperature are explained by the season during the sampling month. Salinity also exhibited consistent high salinity at the mouth of Galveston Bay and decreased towards Trinity Bay and the Lower San Jacinto during each sampling period. November had the highest overall salinity throughout the bay, consistent with the dry season in Texas and low flow rates from Trinity River (Orlando, 1993). Sampling occurred at each station predominantly during ebb tide. This can explain the overall low salinity in the bay and the highest observed salinity of 20.8. Overall, Galveston Bay is well oxygenated, as surface dissolved oxygen (DO) never fell to hypoxic levels of 0.8 mM or below. Since gas solubility increases with decreasing temperatures, the higher DO values in March and November compared to June and September observed are expected. DO levels decreased from the fresher water in the rivers, bayous, and Lower San Jacinto to the mouth of Galveston Bay and higher salinity values.

Concentrations of nitrate (NO_3^-), nitrite (NO_2^-), ammonium (NH_4^+), and phosphate (HPO_4^{2-}) were highest in Buffalo Bayou, San Jacinto River, Trinity River, and the Lower San Jacinto region for all sampling months. The relative high concentration of nutrients leads to the lower DO values observed in these regions, as higher nutrient values tend to increase biological activity. However, in March 2019, NO_3^- had values of

zero μM at station 3, 5, 14, and 13. Whether this is a natural phenomenon or a result of the ITC fire is unknown.

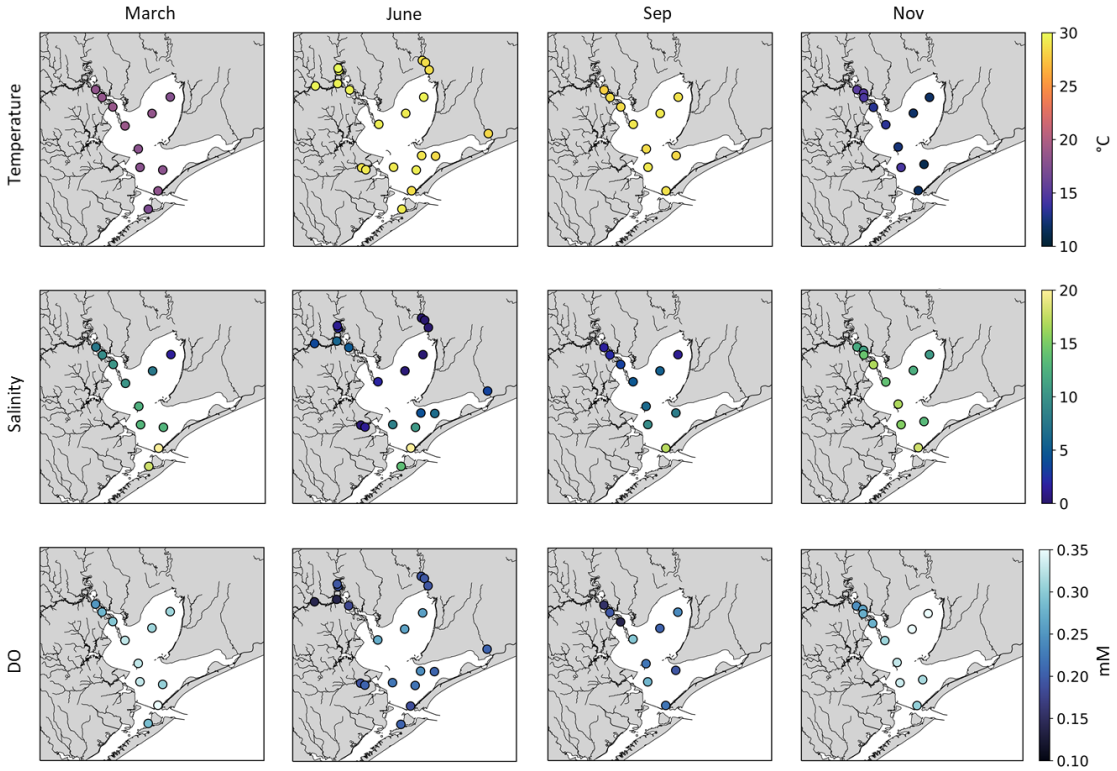

Figure 9: Surface Temperature (°C), Salinity, and DO (mM) for the months of March, June, September, and November 2019 for stations sampled in Galveston Bay.

Discharge rates (m^3 s^{-1}) came from water gauges operated and maintained by the United States Geological Survey (USGS) for the two primary freshwater injection paths (Trinity River and San Jacinto River/Buffalo Bayou) responsible for ~90% of the freshwater inflow. The three gauges chosen were USGS 08070200 in New Caney, TX for the San Jacinto River, USGS 08066500 in Romayor, TX for the Trinity River, and USGS 08074000 in Houston, TX for Buffalo Bayou. For the sampling periods and dates, little to no discharge data collected for Buffalo Bayou, so the importance of flow rate

from this bayou is hard to determine (Figure 10, Table 3). A high-flow event occurred due to rainfall from Tropical Storm Imelda for both Buffalo Bayou and San Jacinto River in September 2019, ten days after the sampling in this study. Overall, Trinity River has a higher discharge rate than the San Jacinto River and Buffalo Bayou and determines the overall salinity content within Galveston Bay (Orlando, 1993; Rayson et al. 2015). Therefore, during the high flow months of March (327.86 $m^3 s^{-1}$) and June (971.65 $m^3 s^{-1}$), Galveston Bay will more reflect the conditions found in Trinity River and by extension Trinity Bay, while the low flow months of Sep (42.87 $m^3 s^{-1}$) and Nov (47.69 $m^3 s^{-1}$) will reflect a mix of oceanic water, San Jacinto River, Buffalo Bayou, and Trinity River.

Table 3: Monthly mean (min-max) flow rate for sampling months in 2019. N/D means no data is available.

Month	Buffalo Bayou	San Jacinto River	Trinity River
March	N/D	5.80 (2.20-16.39)	327.86 (139.90-529.60)
June	N/D	5.06 (0.98-24.53)	971.65 (815.63-1325.40)
Sep	N/D	43.86 (0.53-979.89)	42.87 (33.70-83.83)
Nov	N/D	2.15 (1.37-8.07)	47.69 (36.82-54.66)

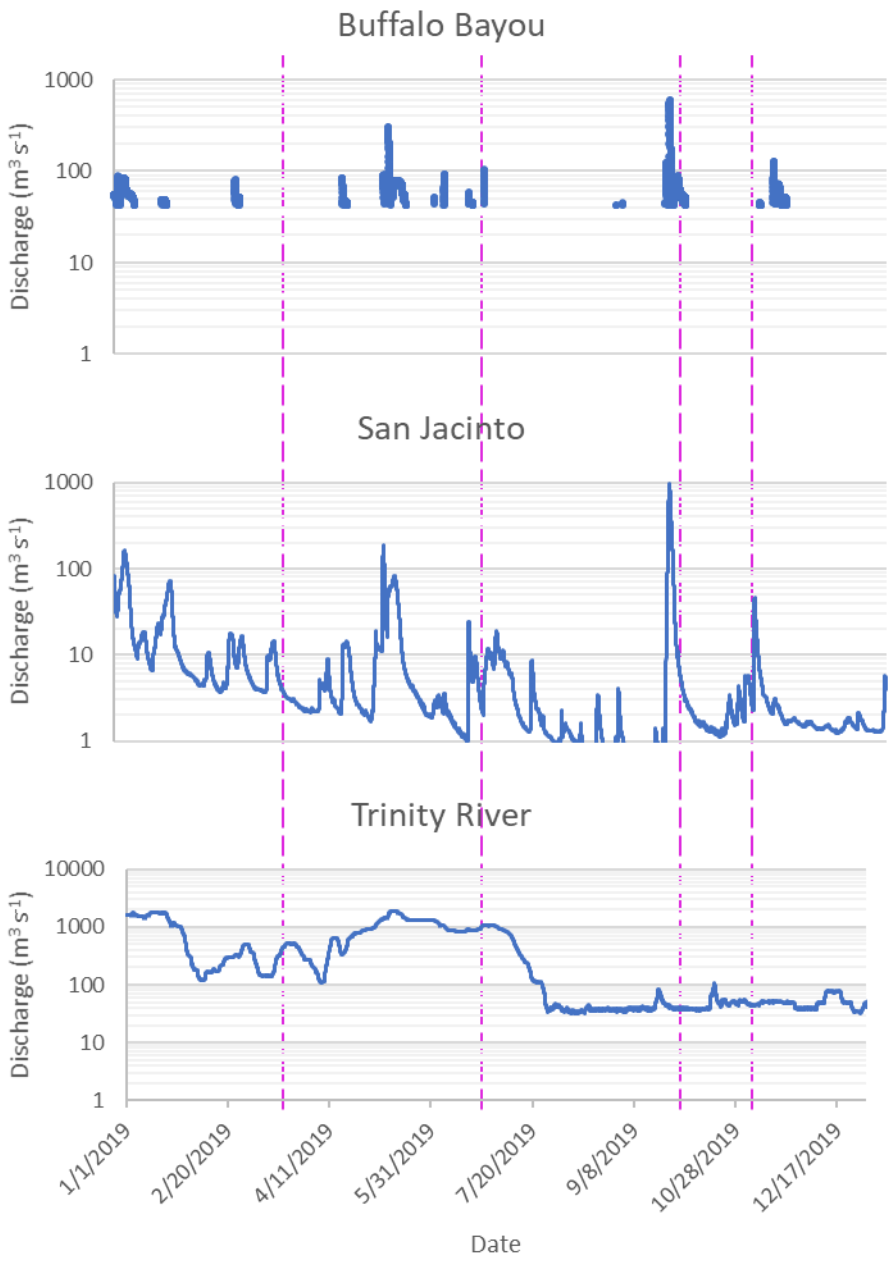

Figure 10: Discharge rates in $m^3 s^{-1}$ in log scale for Buffalo Bayou, San Jacinto, and Trinity River the 2019. Purple lines mark cruise dates in March, June, September, and November. June is representative of both the endmember cruises (June 15-16, 2019) and the Galveston Bay cruise (June 19, 2019). No data exists below 40 $m^3 s^{-1}$ for Buffalo Bayou.

6.2. Water Concentration and Distribution

Overall, the spatial distribution of CCl_4, CFC-11, $CHCl_3$, and PCE is consistent across all months during the sampling period (Figure 11). No data exist for CCl_4 for September due to a contamination issue. The highest concentrations for all compounds are at Station 20 near the confluence of Buffalo Bayou and the San Jacinto River and decreases until reaching Upper Galveston Bay. In the high flow months of Trinity River (March and June), concentrations in Upper Galveston Bay, Lower Galveston Bay, and Trinity Bay show little to no spatial variation within the Bay itself for CCl_4, CFC-11, and PCE (Table 4, 6, 7). West Bay exhibits potentially increased concentrations of CCl_4 and CFC-11. However, it is hard to determine the importance of this from only one station sampled in this region two out of the four cruise dates. September data follow similar trends as the low flow months for spatial concentration distribution within all of Galveston Bay for all compounds. In November, elevated concentrations of CCl_4, CFC-11, and PCE are observed in every sub bay compared to previous month. The colder water temperatures in November (< 15.2 °C) compared to June and September (> 27.9 °C) could lead to increased concentrations of anthropogenic HVOCs in the water due to the increase in gas solubility in colder waters.

Overall, outside of June, Upper Galveston Bay concentrations of $CHCl_3$ are 2 – 17 times higher than Lower Galveston Bay, West Bay, and Trinity Bay (Table 5). In the Lower San Jacinto, $CHCl_3$ is at least 1 – 2 orders of magnitude higher in concentration

than the rest of the bay, and therefore mixing processes within Upper Galveston Bay may not dilute $CHCl_3$ effectively. $CHCl_3$ is also more soluble in water than CCl_4, CFC-11, and PCE and may remain in the water longer with or without the flow rate of Trinity River playing much of a factor. PCE is an order of magnitude higher in all sub-bays except West Bay in November compared to March, June, and September.

During the freshwater endmember cruises in June, the range of concentrations for all HVOCs were higher in Buffalo Bayou and the San Jacinto River than all Galveston Bay concentrations ranges except for the Lower San Jacinto Region (Table 8). Therefore, most anthropogenic input of these compounds into Galveston Bay is due to activity in Houston, TX, that enters and flows through the Lower San Jacinto. Other freshwater inputs of note are Dickenson Bayou for $CHCl_3$ (38.87 – 175.15 pM) and East Bay/Oyster Bayou for PCE (5.88 – 7.33 pM). Industrial cleaning services are in the Dickensen Bayou area. If chlorination or a chlorinated solvent is the primary cleaning agent, then input through wastewater could explain the observed increase. The observed increase in PCE in East Bay/Oyster Bayou is of unknown origin. While PCE is a potential natural product by some macroalgae (Abrahamsson et al., 1995), a five times higher concentration than the other sub bays require an anthropogenic source.

To determine spatial correlations within Galveston Bay between HVOCs, nutrients, and other parameters, Spearman rank correlation coefficients were used. Spatially, PCE and $CHCl_3$ show significant correlations ($p < 0.05$) for the months of March ($r = 0.818$), September ($r = 0.673$), and November ($r = 0.700$). $CHCl_3$ also correlates well with NO_3^-, HPO_4^{2-}, and NH_4^+ in June, September, and November, most

likely due to $CHCl_3$ being a common byproduct in wastewater chlorination. Of note is that CCl_4 and CFC-11 only show a significant correlation in March ($r = 0.609$), leading to the conclusion that they potentially have different loss mechanisms or source locations in this region. No other significant correlations for nutrients and HVOCs can be determined.

Per- and polyfluorinated alkyl substances (PFAS) are a class of compounds that contain over a thousand chemicals (OECD, 2019). Banned eight carbon chain PFAS chemicals found in waterways and sediments are perfluorooctanoic acid (PFOA), used to make Teflon and other chemicals as a feedstock and perfluorooctanesulfonic acid (PFOS), a key ingredient in Scotchgard. 6:2 fluorotelomer sulfonate (6:2 FTS) is a surfactant used in air firefighting foams (AFFFs). Perfluorobutanesulfonic acid (PFBS), a four-carbon chain PFAS chemical, is the current replacement compound used in place of PFOS. Using these compounds as tracers can determine three potential source locations: legacy pollution or landfill sites (PFOS and PFOA), water contaminated from firefighting efforts in the area (6:2 FTS), and current outfall sources (PFBS). Using Spearman rank correlation, CCl_4 and CFC-11 show significant correlation ($p < 0.05$) with PFOA in March ($r = 0.656$ and 0.761, respectively) and June ($r = 0.536$ and 0.561, respectively). There was no correlation with any PFAS chemicals in September. This could be explained by Tropical Storm Imelda, with the freshwater infusion potentially affecting the concentration of the source of PFOA into the bay. PCE correlated with PFOS in March ($r = 0.695$) and June ($r = 0.566$). Potential banks of PFOS could exist in regions where PCE is used and enters the waterways of Galveston Bay, TX. No

compounds correlated with PFBS except for CFC-11 in June ($r = -0.617$). Therefore, HVOCs measured in this study could have sources that are different from PFAS in the bay. While significant correlations existed for all compounds with 6:2 FTS, this compound only appeared in the Lower San Jacinto region and is most likely driving the correlation. Therefore, no conclusions can be drawn from 6:2 FTS use with sources of HVOCs into the bay.

The effects of the ITC Fire in Deer Park, TX in March 2019, and Tropical Storm Imelda in September 2019 did not appear to affect the concentrations of the HVOCs in this study in Galveston Bay. While low concentrations are observed in the low flow Trinity River month of September, the inherently low flow of the Lower San Jacinto region may not have influenced the concentration of HVOCs in the bay directly following a wet season. While over 39" of rain dropped in the surrounding Galveston Bay watershed a week before sampling, little effect was noticed temporally than the other sampling months. However, this is not to say they did not have an effect. This is the first initial study to determine the concentration of these HVOCs in Galveston Bay, so a longer time series is needed to understand and quantify normal conditions in March and September without the effects of any natural or anthropogenic events.

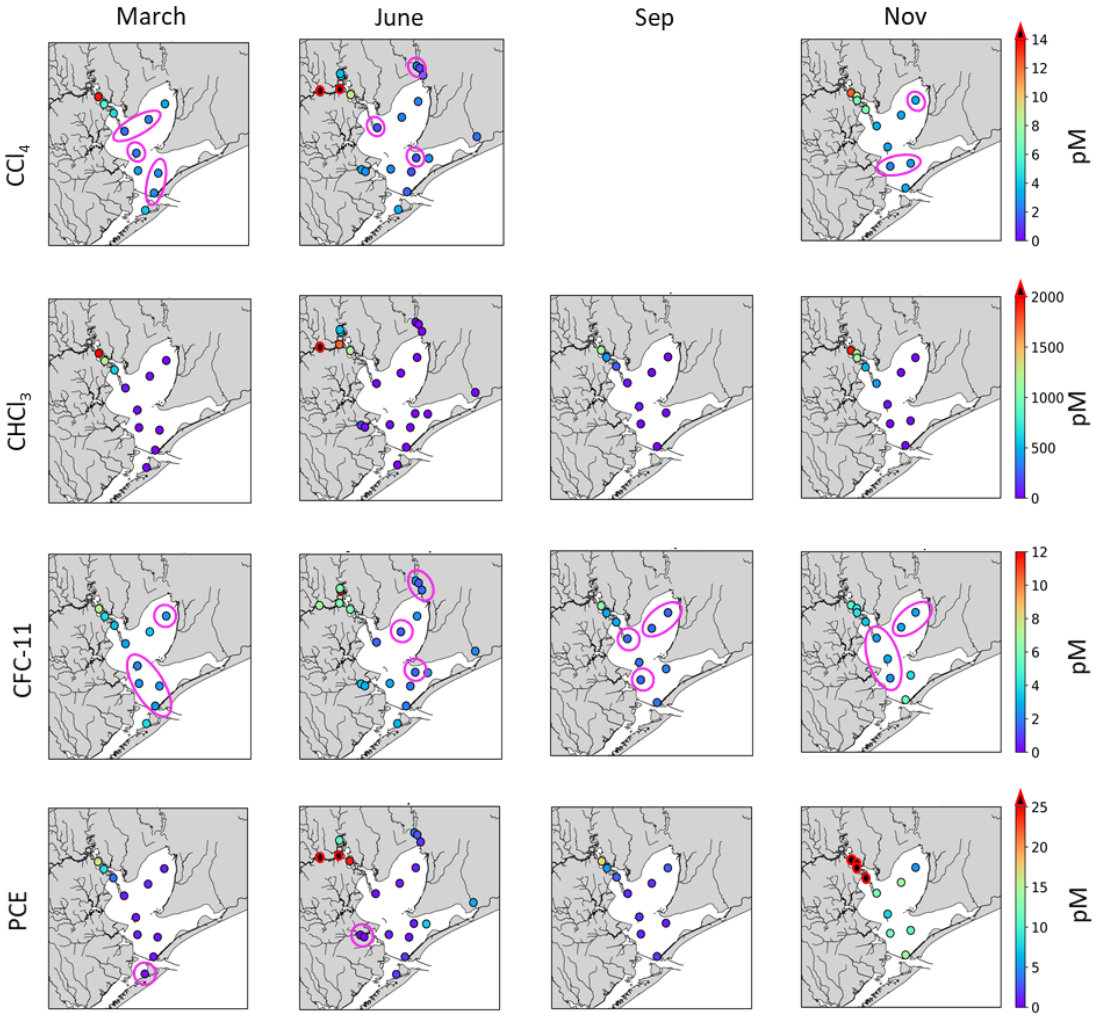

Figure 11: Distribution of water concentrations (pM) of CCl_4, $CHCl_3$, CFC-11, and PCE for March, June, September, and November of 2019. Stations circled in pink have a negative saturation anomaly. All other stations have a positive saturation anomaly. Stations that are a black and red circle are higher values than the color bar. No data is shown for CCl_4 in September due to a contamination issue.

Table 4: Range of concentrations (pM) for each region for CCl_4.

Region	Stations	March	June	Sep	Nov
Upper Galveston Bay	13, 14	1.99-2.35	1.43*	N/D	3.27-3.52
Lower Galveston Bay	9, 11, 5B, 5A	2.64-3.11	1.30-2.56	N/D	2.39-3.24
West Bay	1	3.98*	3.40*	-	-
Trinity Bay	9, 12	2.40-3.34	2.31-2.44	N/D	3.12-3.40
Lower San Jacinto	20, 21, 22, H1	4.51-13.52	8.79*	N/D	6.74-12.15

*Only one station from area sampled
N/D: None Detected
-: No Sampling in Region

Table 5: Range of concentrations (pM) for each region for $CHCl_3$.

Region	Stations	March	June	Sep	Nov
Upper Galveston Bay	13, 14	96.45-114.27	16.3*	60.75-70.06	55.43-420.80
Lower Galveston Bay	9, 11, 5B, 5A	14.55-20.58	6.57-32.92	14.10-36.64	9.15-21.65
West Bay	1	16.71*	17.80*	-	-
Trinity Bay	9, 12	15.33-42.66	10.48-12.35	22.81-29.55	15.89-29.82
Lower San Jacinto	20, 21, 22, H1	598.91-2040.60	1182.54*	237.11-1147.37	504.56-1910.04

*Only one station from area sampled
N/D: None Detected
-: No Sampling in Region

Table 6: Range of concentrations (pM) for each region for CFC-11.

Region	Stations	March	June	Sep	Nov
Upper Galveston Bay	13, 14	2.12-2.64	1.52*	1.69-1.82	2.53-2.81
Lower Galveston Bay	9, 11, 5B, 5A	2.40-2.49	2.00-2.85	1.57-1.96	2.33-5.65
West Bay	1	3.88*	2.99*	-	-
Trinity Bay	9, 12	2.48-3.40	1.49-2.39	1.54-1.66	2.74-2.77
Lower San Jacinto	20, 21, 22, H1	3.25-7.28	2.98*	2.72-6.31	3.40-5.15

*Only one station from area sampled
N/D: None Detected
-: No Sampling in Region

Table 7: Range of concentrations (pM) for each region for PCE

Region	Stations	March	June	Sep	Nov
Upper Galveston Bay	13, 14	0.78-0.98	0.51*	1.48-1.73	7.69-12.22
Lower Galveston Bay	9, 11, 5B, 5A	0.40-1.05	0.64-1.60	0.88-1.77	10.69-14.22
West Bay	1	N/D*	2.00*	-	-
Trinity Bay	9, 12	1.05-1.42	1.14-1.20	1.53-3.03	4.97-13.98
Lower San Jacinto	20, 21, 22, H1	3.60-16.55	24.06*	3.11-17.20	28.34-56.27

*Only one station from area sampled
N/D: None Detected
-: No Sampling in Region

Table 8: Concentration ranges for all compounds during endmember cruise in June 2019. All concentrations are in pM.

Region	Stations	CCl4 (pM)	CHCl3 (pM)	CFC-11 (pM)	PCE (pM)
Dickenson Bayou	101, 103	2.78-3.24	38.87-175.15	2.98-3.34	N/D
Buffalo Bayou	201, 202	23.05-23.66	1735.51-2721.75	6.12-6.73	51.47-72.14
San Jacinto River	301, 302	3.75-4.45	542.82-675.72	6.12-11.82	10.62-17.37
East Bay/Oyster Bayou	401, 402	2.04-2.67	10.89-15.61	2.10-2.55	5.88-7.33
Trinity River	501, 502, 503	1.28-2.33	15.57-24.98	1.43-2.55	1.58-3.43

6.3. Atmospheric Concentration

The atmospheric concentrations of CCl_4 and CFC-11 showed similar trends spatially during each sampling cruise (Table 9). The highest values observed for CCl_4 are in March following the ITC Fire and the concentrations decreased each following month. All months are below the current northern hemisphere (NH) average of CCl_4 of 77.7 ppt, extracted from the Advanced Global Atmospheric Gases Experiment (AGAGE). The air concentrations of CCl_4 measured during the sampling period are less than observed by Hu et al. (2016), where values as high as 500 ppt for CCl_4 were observed in the Houston, TX area over repeated measurements from aircraft and ship campaigns. Air concentrations for CFC-11 over Galveston Bay were equal to or lower than the NH average of 230 ppt for all months sampled (Table 9).

Wing from a southern direction over the Deer Park region of metropolitan area of Houston, TX can lead to higher CCl_4 concentrations observed in northern Houston (Smith et al., 2007). Therefore, it can be assumed that a NW wind over Houston may lead to a higher concentration of CCl_4 over Galveston Bay. Wind direction data was obtained from Station GNJT2, a meteorological station maintained by NOAA's National Data Buoy Center (NDBC) along the Bolivar Roads at the mouth of Galveston Bay. Only sampling performed during March 24th (SE wind) and June 19th (SW wind) had wind directions that did not arrive from a NW direction from Houston, TX to Galveston Bay. However, no significant difference in or increase in CCl_4 atmospheric concentration was observed (Table 9).

PCE concentrations were above the NH average mean of 2.0 ppt measured by AGAGE at all sampling stations in June, September, and November 2019 (Table 9). Values increased throughout the year of sampling, with the highest monthly values in June and November observed in air flasks collected in the Lower San Jacinto region. The atmospheric concentrations of $CHCl_3$ are between 40.4% and 206.7% of the NH mean of 14.6 ppt. The highest concentration observed at Dickenson Bayou in June (30.18 ppt), at the mouth of Galveston Bay in September (10.74 ppt), and the Lower San Jacinto in November (20.27 ppt) (Table 9). The lowest $CHCl_3$ concentrations were in Trinity Ba. As the Trinity River's flow rate (> 850 m^3 s^{-1} in June) can dominate the salinity and, therefore, composition of Galveston Bay (Rayson et al. 2015), biological production of $CHCl_3$ was not as high as has been observed in coastal ocean areas dominated by diatoms and macroalgae (He et al., 2013).

Table 9: Average air concentrations with range for all compounds. March data obtained from TCEQ. N/D means no data.

	March	June	Sep	Nov
CCl_4	77.	65.3 (60.9-70.0)	61.7 (60.8-62.9)	58.8 (57.0-59.9)
$CHCl_3$	10.	11.5 (5.90-30.2)	8.67 (7.24-10.7)	16.1 (11.5-20.3)
CFC-11	230.	211. (206.-218.)	207. (204.-210.)	226. (215.-236.)
PCE	N/D	2.87 (2.04-5.49)	6.06 (5.98-6.16)	8.53 (6.29-11.4)

6.4. Air-Sea Flux and Saturation Anomaly

Air-sea exchange between the atmosphere and ocean is controlled by many thermodynamic and kinetic forcing factors (Wanninkhof et al., 2009). The thermodynamic factors (water temperature, transport, and biological factors) control the difference in concentration between the atmosphere and water. Therefore, these factors do not necessarily need to be accounted for, as the difference in air and water concentration of the gas already considers these. The kinetic forcing factors control the gas transfer velocity (k_w), which currently has only been quantified empirically (Wanninkhof et al., 2009). The kinetic factors contributing are wind speed, surface friction velocity in water, slope, and boundary layer dynamics, with several variables contributing. However, wind speed is the variable used to derive k_w for the ocean empirically. Current equations to calculate k_w lead to only a 20% error in flux calculations (Wanninkhof, 2014).

While Wanninkhof (2014) is the accepted equation in open ocean studies, other water bodies have no consensus equation to calculate k_w. Although wind speed is a good

proxy, it does not consider the increased organic matter, tidal current, or shallow depth that could play a role in flux to and from the water (Abril et al., 2009; Borges et al., 2004). Estuary calculations for k_w consider that the parameters controlling k_w could be different for each estuary, and therefore studies must be done to determine whether they are viable in multiple situations (Abril et al., 2009; Borges et al., 2004; Jiang et al, 2008). For this study, six equations were examined to calculate the flux of each gas in Galveston Bay (Table 10). The equation put forth by Jiang et al. (2008) was selected to explain the flux of gases in Galveston Bay:

$$k_{600} = 0.314u_{10}^2 - 0.436u_{10} + 3.990$$

where k_{600} is the gas transfer velocity of CO_2 (cm hr^{-1}), and u_{10} is the wind speed measured at 10 m height (m s^{-1}). Though wind speed is the only parameter used to derive kw empirically, it was developed using data from fifteen rivers, estuaries, and fjords utilizing three different flux measurement techniques to create a universal estuary k_w equation (Jiang et al., 2008). Wind speed for each sampling period is obtained from Station GNJT2, a meteorological station maintained by NOAA's National Data Buoy Center (NDBC) along the Bolivar Roads at the mouth of Galveston Bay.

Table 10: Air-sea flux equations examined for this study. k_{600} is the gas transfer velocity (cm hr^{-1}), SA is the surface area of the estuary (km^2), TSS is total suspended solids (g L^{-1}), *u* is the measured wind speed at 10m height (m s^{-1}), w is the water current velocity (m s^{-1}), h is the max depth of the estuary/water body (m), and S is the slope of the river (unitless).

Source	Equation	Defined Use-Case
Abril et al., 2009	$k_{600} = 1.80e^{-0.0165w} + (1.23 + 1.00\log(SA)) * (1 - 0.44TSS)u$	Macrotidal estuary
Borges et al., 2004	$k_{600} = 1.0 + 1.719w^{0.5}h^{-0.5}\ 2.58u$	Estuaries/Fjords
Crusius and Wanninkhof, 2003	$k_{600} = 0.228u^{2.2} + 0.168$	Small, shallow lake
Jiang et al., 2008	$k_{600} = 0.314u^2 - 0.436u + 3.990$	Estuaries
Raymond et al., 2012	$k_{600} = (wS)^{0.89} * h^{0.54} * 5037$	Rivers and streams
Wanninkhof, 2014	$k_{600} = 0.251u^2$	Ocean

k_{600} is determined initially for carbon dioxide (CO_2) in most studies, with oxygen (O_2) used for some river studies (Raymond et al., 2012). To determine the k_w for a specific gas:

$$k_w = k_{600}\left(\frac{Sc}{600}\right)^{-n}$$

where Sc is the Schmidt number of the gas (unitless), k_{600} is the gas transfer velocity of CO_2 (m s^{-1}), k_w is the gas transfer velocity of the HVOC (m s^{-1}), and n is the Schmidt number exponent that is either 0.5 to 0.67 depending on the surface state of the water or the wind speed (Wanninkhof et al., 2009; Raymond et al., 2012). In general, all estuarine and river k_{600} are normalized to 600 which corresponds to the Schmidt number of CO_2 and O_2 in fresh water at 20° C and 17.5° C respectively (Raymond et al., 2012). The Schmidt number is calculated for each gas and considers the effect of the kinematic

viscosity of the water, therefore the temperature and salinity, and the diffusivity of the gas on air-sea exchange.

Flux is calculated by the equation:

$$F = k_w([g]_{water} - K_{H,gas}X_{gas})$$

where F is the sea-to-air flux of the gas for the sea surface (mol m^{-2} day^{-1}), $[g]_{water}$ is the concentration of the HVOC in the water (pM), $K_{H,gas}$ is the solubility coefficient of the HVOC, and X_{gas} is the partial pressure of the HVOC in the atmosphere (patm). A positive flux means the gas is emitted from the ocean to the atmosphere to achieve equilibrium, while a negative flux means that the gas is intruding into the ocean from the atmosphere to achieve equilibrium.

Saturation anomaly is the percent above or below equilibrium water concentration of a gas is in relation to the atmospheric concentration of the same gas. A positive saturation anomaly means that the water is supersaturated with the gas and suggests an source outside of the atmosphere to the water. A negative saturation anomaly for a gas means that an overall loss within the water column occurs outside of air-to-sea flux and is undersaturated. Saturation anomaly is calculated by the equation:

$$Saturation\ Anomaly\ (\%) = \left(\frac{[g]_{water} - K_{H,gas}X_{gas}}{K_{H,gas}X_{gas}}\right) X\ 100$$

where $[g]_{water}$ is the gas concentration in the water in mol L^{-1}, $K_{H,gas}$ is the solubility coefficient of the gas in mol L^{-1} atm^{-1}, and X_{gas} is the partial pressure of the gas in atm. For the saturation anomalies in Galveston Bay, the average air concentration for each gas in each month was used (Table 9). Solubility coefficients of CCl_4 and CFC-11 were

calculated using solubility equations from Bullister and Wisegarver (1998) and Warner and Weiss (1985), respectively. Solubility coefficients and $CHCl_3$ and PCE were calculated using solubility equations from Moore (2000) with a salt-out coefficient applied from Gossett (1987).

Sea-to-air flux values are an average of all stations in the specified section (Tables 11-14). Emission values are calculated from the average flux and the surface area of the region. Galveston Bay is not split into the specific sub bays. For CCl_4 and CFC-11 in Galveston Bay, the temporal variation was similar with the highest positive flux in June and overall negative flux in March and November (Tables 11, 13). There was a positive flux in September for CFC-11 as well. The atmospheric concentration is the highest for both compounds in March and for CFC-11 in November, however it is lowest in November for CCl_4 (Table 9). As the waters of Galveston Bay in March and November are cooler by at least 10 °C, temperature of the water could play a significant role in flux for these HVOCs. If we assume the temperature of the waters of Galveston Bay are 15 °C in June instead of over 29 °C, an average negative flux of -2.78 nmol m^{-2} d^{-1} and -3.62 nmol m^{-2} d^{-1} would have occurred for CCl_4 and CFC-11, respectively. This suggests that a potential source of these banned HVOCs is occurring in Galveston Bay, with sea surface temperature (SST) dictating whether there is a positive or negative flux.

$CHCl_3$ and PCE exhibit positive flux and emission across all sampling periods in Galveston Bay (Table 12, 14). The highest flux is in September (76.83 nmol m^{-2} d^{-1}) and November (64.78 nmol m^{-2} d^{-1}) for $CHCl_3$ and November (6.89 nmol m^{-2} d^{-1}) for PCE. The lowest flux occurred in March for both compounds, with a flux of 52.18 and 0.81

nmol m^{-2} d^{-1} respectively. Unlike the banned HVOCs, $CHCl_3$ and PCE appear to not be affected by temporal temperature variations. The reason for the observed highs and lows are unknown, but they suggest potential for uneven sources temporally into Galveston Bay.

The Lower San Jacinto region is roughly 2.3% the size of Galveston Bay. Emission (Gg yr^{-1}) for all compounds from the Lower San Jacinto region is on the same or one less order of magnitude than Galveston Bay emissions (Tables 11-14). In some cases, higher emissions in the Lower San Jacinto region than Galveston Bay occurred for CCl_4 in March and November, CFC-11 in March, September, and November, and $CHCl_3$ in March and June. PCE emission values for the Lower San Jacinto Region were all below Galveston Bay emission. Coupled with the water concentrations observed in this area, significant anthropogenic sources of all compounds must occur for the observed flux and emission from the Lower San Jacinto.

The emissions from parts of Buffalo Bayou and the San Jacinto River, roughly 0.26% and 0.25% the surface area of Galveston Bay in this study, are on the same or one less order of magnitude as Galveston Bay for all compounds in June (Tables 11-14). The only exception is the emission of CCl_4 from the San Jacinto River, which is two orders of magnitude less (Table 11). These high flux rates and emissions spatially correlate to water concentration values. However, increases in atmospheric concentration in this area do not appear to be affected significantly. Flux of all compounds from the sea to air in Buffalo Bayou, San Jacinto River, and the Lower San Jacinto Region is a potentially significant removal process of these compounds.

There are negative saturation anomalies throughout Galveston Bay for CCl_4 and CFC-11 in March and November, and September for CFC-11 (Tables 11, 13), with negative saturation anomalies observed in Upper Galveston Bay and Lower Galveston Bay for CCl_4, and Upper Galveston Bay, Lower Galveston Bay, and Trinity Bay in June. Negative saturation anomalies exist in Trinity River as well for CCl_4 and CFC-11 (Table 14). Therefore, it can be assumed that the overall composition of the bay is dictated by Trinity River and tidal oceanic water. The water concentrations observed in the Lower San Jacinto, San Jacinto River, and Buffalo Bayou dilute through mixing processes upon entry into Galveston Bay and play little roll in the overall composition of Galveston Bay. PCE and $CHCl_3$ have both positive flux and saturation anomaly values across all stations and months, however the saturation anomalies suggest the dominant source is from the Trinity River into Galveston Bay (Tables 12, 14).

Table 11: CCl_4 flux and emission in Galveston Bay, the Lower San Jacinto, Buffalo Bayou, and San Jacinto River regions.

Location	Size (km^2)	March				June				September				November			
		Flux (nmol m^{-2} d^{-1})	Emission (Gg yr^{-1})	Saturation Anomaly (%)	n	Flux (nmol m^{-2} d^{-1})	Emission (Gg yr^{-1})	Saturation Anomaly (%)	n	Flux (nmol m^{-2} d^{-1})	Emission (Gg yr^{-1})	Saturation Anomaly (%)	n	Flux (nmol m^{-2} d^{-1})	Emission (Gg yr^{-1})	Saturation Anomaly (%)	n
Galveston Bay	1360	-0.34	-2.59E-05	-7.28	8	1.70	1.30E-04	40.88	8	N/D	N/D	N/D	N/D	-3.45E-03	-2.64E-07	0.27	7
Lower San Jacinto	31.5	9.15	1.62E-05	163.84	3	39.39	6.96E-05	485.48	1	N/D	N/D	N/D	N/D	6.42	1.14E-05	213.60	4
Buffalo Bayou	3.57	N/D	N/D	N/D	N/D	120.31	2.28E-05	1405.34	2	N/D	N/D	N/D	N/D	N/D	N/D	N/D	N/D
San Jacinto River	3.37	N/D	N/D	N/D	N/D	14.22	2.85E-06	163.43	2	N/D	N/D	N/D	N/D	N/D	N/D	N/D	N/D
Total			-9.69E-06				2.00E-04				N/D				1.11E-05		

Table 12: $CHCl_3$ flux and emission in Galveston Bay, the Lower San Jacinto, Buffalo Bayou, and San Jacinto River regions.

Location	Size (km^2)	March				June				September				November			
		Flux (nmol m^{-2} d^{-1})	Emission (Gg yr^{-1})	Saturation Anomaly (%)	n	Flux (nmol m^{-2} d^{-1})	Emission (Gg yr^{-1})	Saturation Anomaly (%)	n	Flux (nmol m^{-2} d^{-1})	Emission (Gg yr^{-1})	Saturation Anomaly (%)	n	Flux (nmol m^{-2} d^{-1})	Emission (Gg yr^{-1})	Saturation Anomaly (%)	n
Galveston Bay	1360	52.18	3.12E-03	4.39E+04	8	58.30	3.48E-03	2.17E+04	8	76.83	4.59E-03	3.91E+04	7	64.78	3.87E-03	9.56E+04	7
Lower San Jacinto	31.5	2640.69	3.65E-03	1.98E+06	3	6682.19	9.24E-03	7.57E+05	1	1592.23	2.20E-03	7.01E+05	3	1379.86	1.91E-03	1.33E+06	4
Buffalo Bayou	3.57	N/D	N/D	N/D	N/D	12868.44	1.91E-03	6.92E+05	2	N/D	N/D	N/D	N/D	N/D	N/D	N/D	N/D
San Jacinto River	3.37	N/D	N/D	N/D	N/D	3563.23	5.59E-04	1.89E+05	2	N/D	N/D	N/D	N/D	N/D	N/D	N/D	N/D
Total			6.77E-03				1.27E-02				6.79E-03				5.78E-03		

Table 13: CFC-11 flux and emission in Galveston Bay, the Lower San Jacinto, Buffalo Bayou, and San Jacinto River regions.

Location	Size (km^2)	March				June				September				November			
		Flux (nmol m^{-2} d^{-1})	Emission (Gg yr^{-1})	Saturation Anomaly (%)	n	Flux (nmol m^{-2} d^{-1})	Emission (Gg yr^{-1})	Saturation Anomaly (%)	n	Flux (nmol m^{-2} d^{-1})	Emission (Gg yr^{-1})	Saturation Anomaly (%)	n	Flux (nmol m^{-2} d^{-1})	Emission (Gg yr^{-1})	Saturation Anomaly (%)	n
Galveston Bay	1360	-0.11	-7.40E-06	-3.42	8	0.89	6.07E-05	24.17	8	0.13	8.71E-06	2.60	7	-0.34	-2.29E-05	-10.67	7
Lower San Jacinto	31.5	3.57	5.63E-06	67.42	3	23.45	3.70E-05	250.65	1	5.62	8.88E-06	119.44	3	1.08	1.70E-06	28.71	4
Buffalo Bayou	3.57	N/D	N/D	N/D	N/D	26.59	4.49E-06	282.16	2	N/D	N/D	N/D	N/D	N/D	N/D	N/D	N/D
San Jacinto River	3.37	N/D	N/D	N/D	N/D	41.22	7.38E-06	428.21	2	N/D	N/D	N/D	N/D	N/D	N/D	N/D	N/D
Total			-1.77E-06				9.77E-05				1.76E-05				-2.12E-05		

Table 14: PCE flux and emission in Galveston Bay, the Lower San Jacinto, Buffalo Bayou, and San Jacinto River regions.

Location	Size (km^2)	March				June				September				November			
		Flux (nmol m^{-2} d^{-1})	Emission (Gg yr^{-1})	Saturation Anomaly (%)	n	Flux (nmol m^{-2} d^{-1})	Emission (Gg yr^{-1})	Saturation Anomaly (%)	n	Flux (nmol m^{-2} d^{-1})	Emission (Gg yr^{-1})	Saturation Anomaly (%)	n	Flux (nmol m^{-2} d^{-1})	Emission (Gg yr^{-1})	Saturation Anomaly (%)	n
Galveston Bay	1360	0.81	6.69E-05	255.81	8	3.54	2.92E-04	846.93	8	2.79	2.29E-04	465.57	7	6.89	5.67E-04	878.36	7
Lower San Jacinto	31.5	17.49	3.33E-05	4699.86	3	126.60	2.41E-04	9428.36	1	20.69	3.94E-05	2765.89	3	43.60	8.31E-05	4257.42	4
Buffalo Bayou	3.57	N/D	N/D	N/D	N/D	335.07	6.83E-05	5.92E+04	2	N/D	N/D	N/D	N/D	N/D	N/D	N/D	N/D
San Jacinto River	3.37	N/D	N/D	N/D	N/D	76.51	1.65E-05	1.40E+04	2	N/D	N/D	N/D	N/D	N/D	N/D	N/D	N/D
Total			1.00E-04				5.33E-04				2.69E-04				6.50E-04		

6.5. Houston Ship Channel Fate and Transport of HVOCs

A two-box model was developed to understand the transport and fate of HVOCs in the Houston Ship Channel in the Lower San Jacinto region (Figure 12). Through this, an equation was developed to determine whether the losses observed of the HVOCs through the Lower San Jacinto region and the Houston Ship Channel were explained by known loss rates. To determine the typical stratification and density of the waters in the Houston Ship Channel, data from Jan. 1st, 2000 to May 31st, 2020 for 38 stations along the HSC were extracted from the TCEQ Clean Rivers Program database. The 38 stations chosen have temperature and salinity data below 3 m along the HSC. Density was calculated using the TEOS-10 equation from data at depth where sampling of both temperature and salinity occurred at the same date and time. To accumulate enough data to determine an average density gradient, two-month bins were used based off the San Jacinto River discharge rates (Figure 13). Even with 20 years of data in two-month bins, most depths have fewer than two data points, with most data collected at the surface above 3 m. Other organizations, such as NOAA and the Texas Water Development Board (TWDB), do not maintain buoys or water collection stations near the HSC.

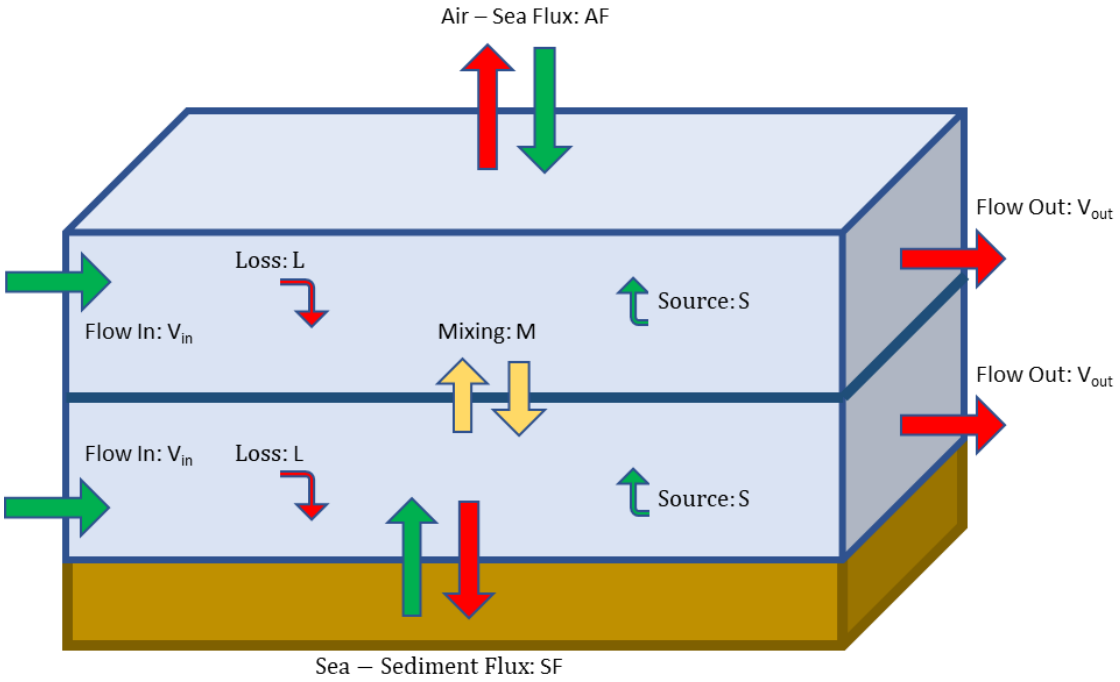

Figure 12: Two-box model of source and loss processes in the Houston Ship Channel for all HVOCs. Red arrows signify a loss of the compound, while green arrows represent a source. Yellow arrows are an unknown source and sink into each box as it is dependent on the concentration of the surface and deep boxes.

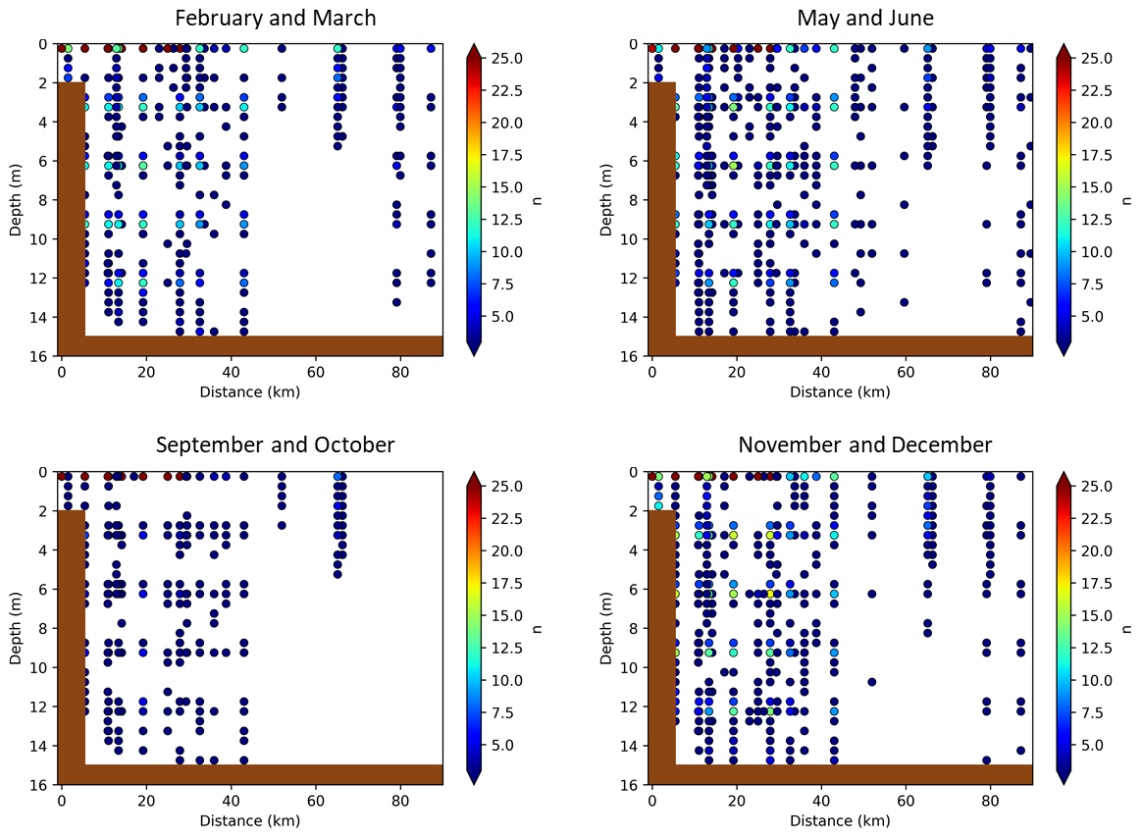

Figure 13: n-values of 2-month bins of data from the TCEQ temperature and salinity value at 0.5 m bin depths at 38 stations across the HSC. Most sampling is at the surface in the Buffalo Bayou/HSC area.

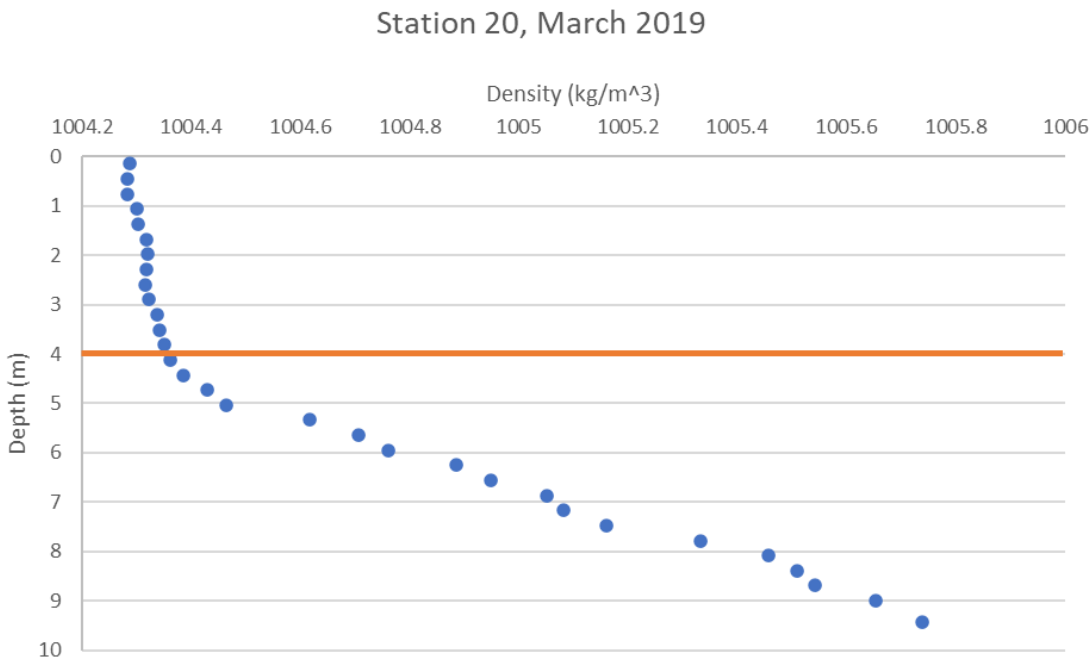

Figure 14: Density profile at Station 20 in March 2019 form Castaway CTD. Surface layer persists to roughly 4 m depth, marked by the red line.

Depth profiles of temperature, salinity, or density of the HSC are limited in the literature. Overall, during peak flood tide, a 2 m surface layer is observed in the Upper Galveston Bay region, while a 6 m deep surface layer exists during peak ebb tide (Schmalz, 2000). However, this sampling is not within the Lower San Jacinto region. The further from the mouth of Galveston Bay and into Upper Galveston Bay and Lower San Jacinto, the stronger the stratification becomes (Schmalz, 2000). One depth profile taken during the March 2019 cruise using a Castaway CTD at station 20 during ebb tide show a 4 m depth of the surface layer in the Lower San Jacinto Region (Figure 14). As

all Lower San Jacinto stations were sampled during ebb tide, a 4 m depth is assumed as the surface layer depth.

Following the potential source and loss parameters of HVOCs in the surface layer from the two-box model, the equation to determine the loss rate of HVOCs in water with time is:

$$[Station] = [Previous] - \left(\left\{\left(k_w([Station] - k_H p_{air}) * \frac{SA}{Vol}\right) + \left(k_z(k_H p_{air} - [Station]) * \frac{SA}{Mid * Vol}\right) + J[Station]\right\} * \frac{u_{water}}{D}\right)$$

where [Station] is the concentration (mol m^{-3}) of the HVOC in the current station, [Previous] is the concentration (mol m^{-3}) of the HVOC of the previous station, k_w is the gas transfer velocity of the HVOC (m d^{-1}), k_H is the Henry's Law coefficient of the HVOC (mol m^{-3} atm^{-1}), p_{air} is the partial pressure of the HVOC in the atmosphere (p_{atm}), SA is the surface area of the Lower San Jacinto between stations (m^2), Vol is the volume of the surface box (m^3), k_z is the eddy diffusivity coefficient (m^2 d^{-1}), Mid is the distance between the center of the boxes (m), J is the rate constant of the HVOC reported in the literature (d^{-1}), u_{water} is the current velocity in the Lower San Jacinto during sampling (m d^{-1}), and D is the distance between the two stations (m). The initial starting concentration is the observed concentration at Station 20 for March, September, and November, and Stations 202 and 302 for June and ending at station H1. For June, through salinity data, it was determined that 77% of the Station 20 water was sourced from Buffalo Bayou, or Station 201, and 23% from the San Jacinto River, or Station 301. The eddy diffusivity

coefficient (k_z) used is 17.28 m^2 d^{-1}, the average k_z of the open ocean. No consensus value exists for estuary vertical diffusivity. As no measured concentrations of HVOCs exist below the surface of the Lower San Jacinto and Houston Ship Channel, the equilibrium value based on Henry's Law is used to serve as a baseline concentration at depth. Assuming the source of the deep water is from the surface or near surface ocean. Rates used for J for each HVOC are in Tables 15-16.

Table 15: Rate constants used for J that include loss through biological degradation and/or particle sequestration

Compound	k (d^{-1})	Region	Source
Carbon Tetrachloride	1.89E-03	Sannich Inlet	Lee et al. (1999)
	3.37E-03	Framvaren Fjord, East Sea	Tanhua and Olsson (2004), Min et al. 2010
CFC-11	9.59E-04	Framvaren Fjord	Tanhua and Olsson (2004)
Chloroform	None	None	
Perchloroethylene	1.01E-04	Delaware River	Ambrose (1987)

Table 16: Rate constants used for J for hydrolysis of the compound for each month from Jeffers et al. (1989).

Compound	Month	k (d^{-1})
Carbon Tetrachloride	March	1.82947E-05
	June	0.000100687
	September	8.77719E-05
	November	9.04127E-06
CFC-11	March	0
	June	0
	September	0
	November	0
Chloroform	March	9.85833E-08
	June	6.14776E-07
	September	5.30557E-07
	November	4.62683E-08
Perchloroethylene	March	6.76459E-12
	June	4.23171E-11
	September	3.65109E-11
	November	3.17069E-12

Figure 15: The projected concentrations of CCl_4 using known loss parameters for March, June, and November 2019. Orange is the observed concentration measured on station, blue is the concentration if flux was the only loss parameter, gray is the concentration if mixing to depth was the only loss parameter, yellow is the concentration if only hydrolysis was the loss parameter, light blue is the concentration from flux and mixing, and green is the concentration from loss with flux, mixing, and the loss rate of CCl_4 at the surface from Tanhua and Olsson (2004).

The loss of CCl_4 observed throughout the Lower San Jacinto in March and November cannot be fully explained by losses to air-sea exchange, mixing to depth, hydrolysis, and reported loss rate constants (Figure 15). While calculated concentrations at Station H1 are with 20% of the observed concentration when considering loss from sea-to-air flux and mixing to depth, Station 21 calculated values are with 40% of observed. CFC-11 exhibits a similar trend as CCl_4 in the months of March, September, and November (Figure 17). While loss parameters are within 20% or statistically the

same in the months of March and September for $CHCl_3$ and PCE at Station H1, November cannot be explained. For $CHCl_3$, the loss by sea-to-air flux and mixing cannot account for the observed concentrations at stations 21, 22, and H1 (Figure 16). An increase in concentration at H1 compared to 22 for PCE suggests a potential source in this region (Figure 18).

Overall, while H1 observed and calculated concentrations are similar for all HVOCs, loss from Station 20 to Station 21 or Station 22 cannot be captured by the current loss parameters in the equation for CCl_4 in March and November, CFC-11 in March, September, and November, $CHCl_3$ in September and November, and PCE in September and November. The Distance between Station 20 to Station 21 is 1302 m, Station 21 to Station 22 is 1790 m, and Stations 22 to H1 is 5288 m. the lack of time for removal between 20, 21, and 22 suggest a potential for another loss or underestimation of loss occurring.

Lack of sampling at Stations 21, 22, and H1 in June limits conclusions that can be drawn on loss in the lower San Jacinto Region of HVOCs. However, the concentration calculated by all combinations of loss parameters besides hydrolysis is lower than observed at Stations 20, 201, and 301 for all compounds (Figures 15-18). This further suggests that Buffalo Bayou and the San Jacinto rivers are sources of these anthropogenic HVOCs into the Lower San Jacinto region before dilution in Upper Galveston Bay. Direct sources are most likely limited into the Lower San Jacinto. However, increased concentrations downstream occurred at H1 for CCl_4 in November, CFC-11 in September, $CHCl_3$ in November, and PCE in November. If there are direct

sources in the LSJ besides Buffalo Bayou and the San Jacinto River, then the loss of each compound is greater than current calculations can account for.

Factors not considered in this model may play a significant role in the loss of anthropogenic HVOCs in this region. It was assumed that the Lower San Jacinto region does not experience tidal influence and continuously flows towards Galveston Bay. The calculations of loss of HVOCs from the surface water due therefore more than likely understate the impacts of calculated. If equations accounted for the added time necessary due to tidal forces, the loss would most likely be greater. This further suggests direct sources of all HVOCs into the Lower San Jacinto region.

Mixing processes between the surface and deep box is presumed to be controlled only through vertical eddy diffusivity in the model. Within the shallow waters of Galveston Bay and the shallow depth of the surface layer of the Houston Ship Channel, wind most likely is a significant factor of mixing to depth. Also, whenever discharge in the Lower San Jacinto region is over 100 $m^3 s^{-1}$, vertical mixing within the Houston Ship Channel occurs (Orlando, 1993). Accounting for these factors would lead to an even greater loss to depth from the surface waters for all HVOCs.

Further loss of HVOCs can occur within the sediment of the Houston Ship Channel. All HVOCs studied can degrade in anaerobic settings in deeper sediment layers. This will lead to a flux of HVOCs from the bottom waters into the sediment, further driving a decreased concentration in the surface waters. Considering all these factors, loss of HVOCs most likely occur at a higher magnitude than currently calculated. Therefore, more direct inputs of anthropogenic HVOCs into the waters of the

Lower San Jacinto are needed to reach the concentrations measured. Further work is needed to understand the sources and sinks of HVOCs in this region.

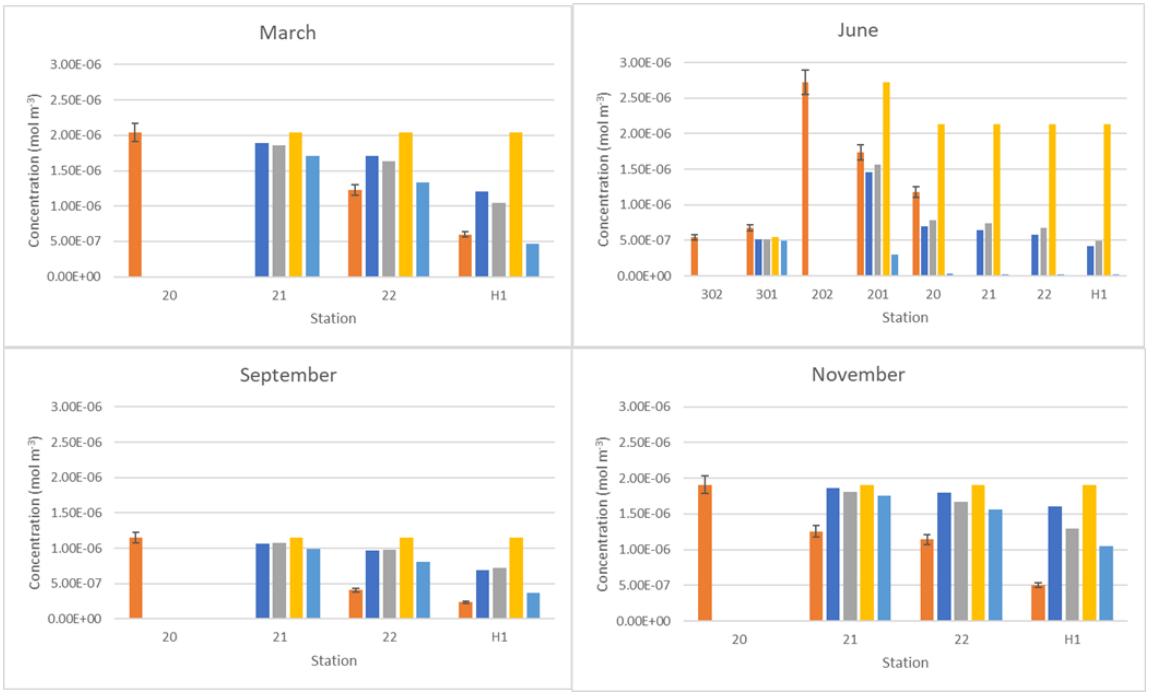

Figure 16: The projected concentrations of $CHCl_3$ using known loss parameters for March, June, September, and November 2019. Orange is the observed concentration measured on station, blue is the concentration if air-sea flux was the only loss parameter, gray is the concentration if mixing to depth was the only loss parameter, yellow is the concentration if only hydrolysis was the loss parameter, and light blue is the concentration from loss by air-sea flux and mixing to depth.

Figure 17: The projected concentrations of CFC-11 using known loss parameters for March, June, September, and November 2019. Orange is the observed concentration measured on station, blue is the concentration if air-sea flux was the only loss parameter, gray is the concentration if mixing to depth was the only loss parameter, yellow is the concentration if only hydrolysis was the loss parameter, light blue is the concentration from loss by air-sea flux and mixing to depth and green is the concentration from loss with flux, mixing, and the loss rate of CFC-11 at the surface from Tanhua and Olsson (2004).

Figure 18: The projected concentrations of PCE using known loss parameters for March, June, September, and November 2019. Orange is the observed concentration measured on station, blue is the concentration if air-sea flux was the only loss parameter, gray is the concentration if mixing to depth was the only loss parameter, yellow is the concentration if only hydrolysis was the loss parameter, green is the concentration from loss by air-sea flux and mixing to depth, and purple is the concentration from loss with flux, mixing, and the loss rate of PCE at the surface from Ambrose (1987).

7. CONCLUSIONS

Elevated concentrations of anthropogenic HVOCs in the Lower San Jacinto region across the sampling period of March, June, September, and November 2019 suggest an anthropogenic source of each compound into the water. However, dilution and mixing of Lower San Jacinto waters into Galveston Bay appear to have little effect on the concentration of each HVOC within the bay itself. The flow of Trinity River plays a large role in the conditions found within the bay. In the high flow months of March and June, the concentrations of all HVOCs found in Upper Galveston Bay, outside of the Lower San Jacinto Region, were similar to Trinity Bay. In the low flow months of September and November, elevated concentrations of $CHCl_3$ and PCE exist in Upper Galveston Bay reflective of the Lower San Jacinto Region. Only $CHCl_3$ and PCE correlate strongly to each other, suggesting common outfall sources in the Lower San Jacinto. Elevated concentrations of CCl_4 and CFC-11 in the Lower San Jacinto, Buffalo Bayou, and the San Jacinto River suggest anthropogenic sources from Houston, TX, however they do not correlate well with each other. This suggests the potential for different sources or loss mechanisms for these banned HVOCs.

Sea-to-air emission of CCl_4, $CHCl_3$, CFC-11, and PCE from the Lower San Jacinto, Buffalo Bayou, and the San Jacinto River are all within one order of magnitude of emission from Galveston Bay during the entire sampling period. The Lower San Jacinto, Buffalo Bayou, and San Jacinto River have surface areas that are 2.3%, 0.26%, and 0.25% the size of Galveston Bay, respectively. Therefore, sea-to-air flux of HVOCs

from the Lower San Jacinto region is a potentially significant loss mechanism to the surface water concentration. However, the air concentrations measured in the Lower San Jacinto region do not reflect an increase flux to the atmosphere. Other sources to the atmosphere may exist for all HVOCs, such as fugitive emissions, in this region.

CCl_4 and CFC-11 have negative saturation anomalies in Trinity River, Trinity Bay, Upper Galveston Bay, and Lower Galveston Bay in June, and throughout Galveston Bay in March, September, and November. Positive saturation anomalies exist throughout the Lower San Jacinto region during the entire sampling period. This suggests that the Trinity River plays a significant role in the CCl_4 and CFC-11 concentrations within the bay itself, and that the high concentrations observed in the Lower San Jacinto region mix and dilute upon entry into Galveston Bay. PCE and $CHCl_3$ have positive saturation anomalies at all stations and regions, however the magnitude is similar to the Trinity River as the major source of these compounds to Galveston Bay over the Lower San Jacinto region.

Throughout the Lower San Jacinto region, unknown sink or sinks occur that cannot be explained through air-sea exchange, vertical mixing processes, or known loss rate constants from biological degradation and particulate sequestration. For this region, and all of Galveston Bay, a sea to air flux rate study is needed to determine the gas transfer velocity equation specific to the region. The large, shallow bay may not be accurately represented by the equation presented by Jiang et al. (2008) for estuaries. Current holistic loss rates that include both biological degradation and particle sequestration for loss in the surface water column are for an oligotrophic basin and a

fjord in Norway and may not represent a well-oxygenated, shallow bay with a deep shipping channel. Furthermore, a large variation in magnitude for vertical eddy diffusivity constants exist in the literature for estuaries, with no value that could apply to an estuary like Galveston Bay. Further work is necessary to understand the physical and biological effects on anthropogenic HVOCs in Galveston Bay to better characterize the fate and transport of these compounds.

This study shows that anthropogenic activity correlates to increased anthropogenic HVOC concentration throughout the Lower San Jacinto region and Galveston Bay. Further study into the sources of HVOCs into Galveston bay are needed to explain elevated concentrations and saturation anomaly throughout the entire region. Sea to air flux cannot explain the loss observed and modeled for all compounds in the Lower San Jacinto region. Further work on a gas transfer velocity equation, vertical mixing processes, and removal rates in Galveston Bay are needed to understand the fate and transfer of each anthropogenic HVOC. The effect of the ITC fire in Deer Park in March 2019 and Tropical Storm Imelda in September 2019 on anthropogenic HVOCs concentration in Galveston Bay is inconclusive based off concentration data and saturation anomaly calculations. While sampling occurred after high freshwater flow from the San Jacinto River and Buffalo Bayou/HSC into Galveston Bay, no conclusions can be drawn from a year's worth of data as no significant variation exists. The ITC fire appears to have made no impact as well, but a longer time series is needed to assess longer term trends and impacts.

REFERENCES

Abrahamsson, K., Ekdahl, A., Collen, J., & Pedersen, M. (1995). Marine algae-a source of trichloroethylene and perchloroethylene. *Limnology and Oceanography*, *40*(7), 1321-1326.

Abril, G., Commarieu, M. V., Sottolichio, A., Bretel, P., & Guerin, F. (2009). Turbidity limits gas exchange in a large macrotidal estuary. *Estuarine, Coastal and Shelf Science*, *83*(3), 342-348.

Amaral, O. C., Otero, R., Grimalt, J. O., & Albaiges, J. (1996). Volatile and semi-volatile organochlorine compounds in tap and riverine waters in the area of influence of a chlorinated organic solvent factory. *Water Research*, *30*(8), 1876-1884.

Ambrose Jr, R. B. (1987). Modeling volatile organics in the Delaware Estuary. *Journal of Environmental Engineering*, *113*(4), 703-721.

Amonette, J. E., Workman, D. J., Kennedy, D. W., Fruchter, J. S., & Gorby, Y. A. (2000). Dechlorination of carbon tetrachloride by Fe (II) associated with goethite. *Environmental Science & Technology*, *34*(21), 4606-4613.

Aucott, M. L., McCulloch, A., Graedel, T. E., Kleiman, G., Midgley, P., & Li, Y. F. (1999). Anthropogenic emissions of trichloromethane (chloroform, CHCl3) and chlorodifluoromethane (HCFC-22): Reactive chlorine emissions inventory. *Journal of Geophysical Research: Atmospheres*, *104*(D7), 8405-8415.

Azetsu-Scott, K., Jones, E. P., & Gershey, R. M. (2005). Distribution and ventilation of water masses in the Labrador Sea inferred from CFCs and carbon tetrachloride. *Marine chemistry*, *94*(1-4), 55-66.

Ballschmiter, K. (2003). Pattern and sources of naturally produced organohalogens in the marine environment: biogenic formation of organohalogens. *Chemosphere*, *52*(2), 313-324.

Brinkmann, T., Santonja, G. G., Schorcht, F., Roudier, S., & Sancho, L. D. (2014). Best available techniques (BAT) reference document for the production of chlor-alkali. *JRC (Joint Research Center EU), JRC91156*.

Bobb, W. H., Boland, R. A. J., & Banchetti, A. J. (1973). Houston ship channel, Galveston Bay, Texas EM dash report 1 Hydraulic and salinity verification.

Boopathy, R. (2002). Anaerobic biotransformation of carbon tetrachloride under various electron acceptor conditions. *Bioresource technology*, *84*(1), 69-73.

Borges, A. V., Delille, B., Schiettecatte, L. S., Gazeau, F., Abril, G., & Frankignoulle, M. (2004). Gas transfer velocities of CO2 in three European estuaries (Randers Fjord, Scheldt, and Thames). *Limnology and Oceanography*, *49*(5), 1630-1641.

Bouwer, E. J., B. E. Rittman, and P. L. McCarty, Anaerobic degradation of halogenated 1- and 2-carbon organic compounds, Environ. Sci. Technol., 15(5), 596-599, 1981.

Bullister, J. L., & Weiss, R. F. (1983). Anthropogenic chlorofluoromethanes in the Greenland and Norwegian Seas. *Science*, *221*(4607), 265-268.

Bullister, J. L., & Wisegarver, D. P. (1998). The solubility of carbon tetrachloride in water and seawater. *Deep Sea Research Part I: Oceanographic Research Papers*, *45*(8), 1285-1302.

Butler, J. H., Battle, M., Bender, M. L., Montzka, S. A., Clarke, A. D., Saltzman, E. S., ... & Elkins, J. W. (1999). A record of atmospheric halocarbons during the twentieth century from polar firn air. *Nature*, *399*(6738), 749-755.

Butler, J., Yvon-Lewis, S., Lobert, J., King, D., Montzka, S., Bullister, J., ... & Liu, Y. (2016). A comprehensive estimate for loss of atmospheric carbon tetrachloride (CCl_4) to the ocean. *Atmos. Chem. Phys*, *16*, 10899-10910.

Carnes, S. A., & Watson, A. P. (1989). Disposing of the US chemical weapons stockpile: an approaching reality. *JAMA*, *262*(5), 653-659.

Carpenter, L. J., S. Reimann, J. B. Burkholder, C. Clerbaux, B. D. Hall, R. Hossaini, J. C. Laube, S. A. Yvon-Lewis, A. Engel, and S. Montzka (2014), Update on ozone-depleting substances (ODSs) and other gases of interest to the Montreal protocol, Scientific assessment of ozone depletion: 2014, 1.1-1.101.

Castro, C. E., Biodehalogenation: The kinetics and rates of the microbial cleavage of carbon-halogen bonds, Environ. Toxicol. Chem., 12, 1609 – 1618, 1993.

Chipperfield, M. P., Liang, Q., Rigby, M., Hossaini, R., Montzka, S. A., Dhomse, S., ... & Salameh, P. K. (2016). Model sensitivity studies of the decrease in atmospheric carbon tetrachloride. *Atmos. Chem. Phys.*, *16*, 15741-15754.

Clark, J. F., Smethie Jr, W. M., & Simpson, H. J. (1995). Chlorofluorocarbons in the Hudson estuary during summer months. *Water Resources Research*, *31*(10), 2553-2560.

Collins, R., & Picardal, F. (1999). Enhanced anaerobic transformations of carbon tetrachloride by soil organic matter. *Environmental Toxicology and Chemistry: An International Journal*, *18*(12), 2703-2710.

Colomb, A., Yassaa, N., Williams, J., Peeken, I., & Lochte, K. (2008). Screening volatile organic compounds (VOCs) emissions from five marine phytoplankton species by head space gas chromatography/mass spectrometry (HS-GC/MS). *Journal of Environmental Monitoring*, *10*(3), 325-330.

Cox, M. L., Sturrock, G. A., Fraser, P. J., Siems, S. T., Krummel, P. B., & O'doherty, S. (2003). Regional sources of methyl chloride, chloroform and dichloromethane identified from AGAGE observations at Cape Grim, Tasmania, 1998–2000. *Journal of Atmospheric Chemistry*, *45*(1), 79-99.

Crusius, J., & Wanninkhof, R. (2003). Gas transfer velocities measured at low wind speed over a lake. *Limnology and Oceanography*, *48*(3), 1010-1017.

Dhomse, S. S., Feng, W., Montzka, S. A., Hossaini, R., Keeble, J., Pyle, J. A., ... & Chipperfield, M. P. (2019). Delay in recovery of the Antarctic ozone hole from unexpected CFC-11 emissions. *Nature communications*, *10*(1), 1-12.

Dyrssen, D., Fogelqvist, E., Krysell, M., & Sturm, R. (1990). Release of halocarbons from an industrial estuary. *Tellus B*, *42*(2), 162-169.

EPA, 2009. National Primary Drinking Water Regulations, EPA 816-F-09-004, <https://www.epa.gov/sites/production/files/2016-06/documents/npwdr_complete_table.pdf> (accessed 11.01.20)

Egli, C., Tschan, T., Scholtz, R., Cook, A. M., & Leisinger, T. (1988). Transformation of tetrachloromethane to dichloromethane and carbon dioxide by Acetobacterium woodii. *Applied and Environmental Microbiology*, *54*(11), 2819-2824.

Egli, C., Stromeyer, S., Cook, A. M., & Leisinger, T. (1990). Transformation of tetra- and trichloromethane to CO2 by anaerobic bacteria is a non-enzymic process. *FEMS Microbiology Letters*, *68*(1-2), 207-212.

Fang, X., Park, S., Saito, T., Tunnicliffe, R., Ganesan, A. L., Rigby, M., ... & Krummel, P. B. (2019). Rapid increase in ozone-depleting chloroform emissions from China. *Nature Geoscience*, *12*(2), 89-93.

Fine, R. A. (2011). Observations of CFCs and SF6 as ocean tracers. *Annual review of marine science*, *3*, 173-195.

Fogel, M. M., Taddeo, A. R., & Fogel, S. A. M. U. E. L. (1986). Biodegradation of chlorinated ethenes by a methane-utilizing mixed culture. *Applied and Environmental Microbiology*, *51*(4), 720-724.

Fraser, P. J., Dunse, B. L., Manning, A. J., Walsh, S., Wang, R. H. J., Krummel, P. B., ... & Simmonds, P. G. (2014). Australian carbon tetrachloride emissions in a global context. *Environmental Chemistry*, *11*(1), 77-88.

Galveston Bay Foundation (2020, September). *Galveston Bay Report Card 2020*. https://www.galvbaygrade.org/wp-content/uploads/2020/09/2020_Galveston_Bay_Full_Report.pdf#page=25

Gossett, J. M. (1987). Measurement of Henry's law constants for C1 and C2 chlorinated hydrocarbons. *Environmental Science & Technology, 21*(2), 202-208.

Graziosi, F., Arduini, J., Bonasoni, P., Furlani, F., Giostra, U., Manning, A. J., ... & Vollmer, M. K. (2016). Emissions of carbon tetrachloride from Europe. *Atmospheric Chemistry & Physics, 16*(20).

Happell, J. D., & Wallace, D. W. (1998). Removal of atmospheric CCl4 under bulk aerobic conditions in groundwater and soils. *Environmental science & technology*, *32*(9), 1244-1252.

He, Z., Yang, G. P., Lu, X. L., & Zhang, H. H. (2013). Distributions and sea-to-air fluxes of chloroform, trichloroethylene, tetrachloroethylene, chlorodibromomethane and bromoform in the Yellow Sea and the East China Sea during spring. *Environmental pollution*, *177*, 28-37.

Hong, H. C., Mazumder, A., Wong, M. H., & Liang, Y. (2008). Yield of trihalomethanes and haloacetic acids upon chlorinating algal cells, and its prediction via algal cellular biochemical composition. *Water Research*, *42*(20), 4941-4948.

Hu, L., Montzka, S. A., Miller, B. R., Andrews, A. E., Miller, J. B., Lehman, S. J., ... & Atlas, E. L. (2016). Continued emissions of carbon tetrachloride from the United States nearly two decades after its phaseout for dispersive uses. *Proceedings of the National Academy of Sciences*, *113*(11), 2880-2885.

Isidorov, V. A. (1990). *Organic chemistry of the earth's atmosphere*.

Jappe, H., Salminen, E., Doddema, H. J., Janssen, D. B., & Harder, W. (1997). Transformation of carbon tetrachloride under sulfate reducing conditions. *Biodegradation*, *8*(6), 429-436.

Jeffers, P. M., Ward, L. M., Woytowitch, L. M., & Wolfe, N. L. (1989). Homogeneous hydrolysis rate constants for selected chlorinated methanes, ethanes, ethenes, and propanes. *Environmental Science & Technology*, *23*(8), 965-969.

Jiang, L. Q., Cai, W. J., & Wang, Y. (2008). A comparative study of carbon dioxide degassing in river-and marine-dominated estuaries. *Limnology and Oceanography*, *53*(6), 2603-2615.

Johnsen, A. R., Jacobsen, O. S., Gudmundsson, L., & Albers, C. N. (2016). Chloroform emissions from arctic and subarctic ecosystems in Greenland and Northern Scandinavia. *Biogeochemistry*, *130*(1-2), 53-65.

Jugder, B. E., Ertan, H., Lee, M., Manefield, M., & Marquis, C. P. (2015). Reductive dehalogenases come of age in biological destruction of organohalides. *Trends in biotechnology*, *33*(10), 595-610.

Jugder, B. E., Ertan, H., Bohl, S., Lee, M., Marquis, C. P., & Manefield, M. (2016). Organohalide respiring bacteria and reductive dehalogenases: key tools in organohalide bioremediation. *Frontiers in microbiology*, *7*, 249.

Khalil, M. A. K., & Rasmussen, R. A. (1993). The environmental history and probable future of fluorocarbon 11. *Journal of Geophysical Research: Atmospheres*, *98*(D12), 23091-23106.

Khalil, M. A. K., & Rasmussen, R. A. (1999). Atmospheric chloroform. *Atmospheric Environment*, *33*(7), 1151-1158.

Koenig, J. C., Lee, M. J., & Manefield, M. (2012). Successful microcosm demonstration of a strategy for biodegradation of a mixture of carbon tetrachloride and perchloroethene harnessing sulfate reducing and dehalorespiring bacteria. *Journal of hazardous materials*, *219*, 169-175.

Krone, U. E., Thauer, R. K., Hogenkamp, H. P., & Steinbach, K. (1991). Reductive formation of carbon monoxide from carbon tetrachloride and FREONS 11, 12, and 13 catalyzed by corrinoids. *Biochemistry*, *30*(10), 2713-2719.

Lakshmanan, D., Howell, N. L., Rifai, H. S., & Koenig, L. (2010). Spatial and temporal variation of polychlorinated biphenyls in the Houston Ship Channel. *Chemosphere*, *80*(2), 100-112.

Mabey, W., & Mill, T. (1978). Critical review of hydrolysis of organic compounds in water under environmental conditions. *Journal of Physical and Chemical Reference Data*, *7*(2), 383-415.

McCulloch, A. (2003). Chloroform in the environment: occurrence, sources, sinks and effects. *Chemosphere*, *50*(10), 1291-1308.

Mendoza, Y., Goodwin, K. D., & Happell, J. D. (2011). Microbial removal of atmospheric carbon tetrachloride in bulk aerobic soils. *Applied and environmental microbiology*, *77*(17), 5835-5841.

Min, D. H., Bullister, J. L., & Weiss, R. F. (2002). Anomalous chlorofluorocarbons in the Southern California Borderland basins. *Geophysical research letters*, *29*(20), 16-1.

Min, D. H., Warner, M. J., & Bullister, J. L. (2010). Estimated rates of carbon tetrachloride removal in the thermocline and deep waters of the East Sea (Sea of Japan). *Marine Chemistry*, *121*(1-4), 100-111.

Molina, M. J., & Rowland, F. S. (1974). Predicted present stratospheric abundances of chlorine species from photodissociation of carbon tetrachloride. *Geophysical Research Letters*, *1*(7), 309-312.

Montzka, S. A., Dutton, G. S., Yu, P., Ray, E., Portmann, R. W., Daniel, J. S., ... & Nance, J. D. (2018). An unexpected and persistent increase in global emissions of ozone-depleting CFC-11. *Nature*, *557*(7705), 413-417.

Moore, R. M. (2000). The solubility of a suite of low molecular weight organochlorine compounds in seawater and implications for estimating the marine source of methyl chloride to the atmosphere. *Chemosphere-Global Change Science*, *2*(1), 95-99.

Mun, T.K., & Kirienko, O. A. (2011). Biodegradation of tri-and perchloroethylene in sewage waters and soils by a microbial consortium of compost and phototrophic bacteria. *Biology Bulletin*, *38*(5), 538.

Nightingale, P. D., Malin, G., & Liss, P. S. (1995). Production of chloroform and other low molecular-weight halocarbons by some species of macroalgae. *Limnology and Oceanography*, *40*(4), 680-689.

Olaniran, A. O., Okoh, A. I., Ajisebutu, S., Golyshin, P., & Babalola, G. O. (2002). The aerobic dechlorination activities of two bacterial species isolated from a refuse dumpsite in Nigeria. *International Microbiology*, *5*(1), 21-24.

Olaniran, A. O., Pillay, D., & Pillay, B. (2004). Haloalkane and haloacid dehalogenases from aerobic bacterial isolates indigenous to contaminated sites in Africa demonstrate diverse substrate specificities. *Chemosphere*, *55*(1), 27-33.

Organization for Economic Co-operation and Development (OECD), To-ward a new comprehensive global database of per- and polyfluoroalkylsubstances (PFASs): Summary report on updating the OECD 2007 list of per-and polyfluoroalkyl substances (PFASs), OECD Ser. Risk Manag. 2018, 2018.http://www.oecd.org/officialdocuments/publicdisplaydocumentpdf/?cote¼ENV-JM-MONO(2018)7&doclanguage¼en. (Accessed 24 August 2020).

Orlando, S. P. (1993). *Salinity characteristics of Gulf of Mexico estuaries*. Strategic Environmental Assessments Division, Office of Ocean Resources Conservation and Assessment, National Ocean Service, National Oceanic and Atmospheric Administration.

Orsi, A. H., Smethie Jr, W. M., & Bullister, J. L. (2002). On the total input of Antarctic waters to the deep ocean: A preliminary estimate from chlorofluorocarbon measurements. *Journal of Geophysical Research: Oceans*, *107*(C8), 31-1.

Park, S., Li, S., Mühle, J., O'Doherty, S., Weiss, R. F., Fang, X., ... & Prinn, R. G. (2018). Toward resolving the budget discrepancy of ozone-depleting carbon

tetrachloride (CCl 4): an analysis of top-down emissions from China. *Atmospheric Chemistry and Physics*, *18*(16), 11729-11738.

Penny, C., Vuilleumier, S., & Bringel, F. (2010). Microbial degradation of tetrachloromethane: mechanisms and perspectives for bioremediation. *FEMS microbiology ecology*, *74*(2), 257-275.

Picardal, F. W., Arnold, R. G., Couch, H., Little, A. M., & Smith, M. E. (1993). Involvement of cytochromes in the anaerobic biotransformation of tetrachloromethane by Shewanella putrefaciens 200. *Applied and Environmental Microbiology*, *59*(11), 3763-3770.

Raymond, P. A., Zappa, C. J., Butman, D., Bott, T. L., Potter, J., Mulholland, P., ... & Newbold, D. (2012). Scaling the gas transfer velocity and hydraulic geometry in streams and small rivers. *Limnology and Oceanography: Fluids and Environments*, *2*(1), 41-53.

Rayson, M. D., Gross, E. S., & Fringer, O. B. (2015). Modeling the tidal and sub-tidal hydrodynamics in a shallow, micro-tidal estuary. *Ocean Modelling*, *89*, 29-44.

Rayson, M. D., Gross, E. S., Hetland, R. D., & Fringer, O. B. (2016). Time scales in Galveston Bay: An unsteady estuary. *Journal of Geophysical Research: Oceans*, *121*(4), 2268-2285.

Ryall, D.B., Derwent, R.G., Manning, A.J., Simmonds, P.G., ODoherty, S., 2001. Estimating source regions of European emissions of trace gases from observations at Mace Head. Atmos. Environ. 35, 2507–2523.

Scheutz, C., Bogner, J., Chanton, J. P., Blake, D., Morcet, M., Aran, C., & Kjeldsen, P. (2008). Atmospheric emissions and attenuation of non-methane organic compounds in cover soils at a French landfill. *Waste Management*, *28*(10), 1892-1908.

Schwarzenbach, R. P., Giger, W., Hoehn, E., & Schneider, J. K. (1983). Behavior of organic compounds during infiltration of river water to groundwater. Field studies. *Environmental science & technology*, *17*(8), 472-479.

Shao, H., & Butler, E. C. (2009). Influence of soil minerals on the rates and products of abiotic transformation of carbon tetrachloride in anaerobic soils and sediments. *Environmental science & technology*, *43*(6), 1896-1901.

Shaver, D. J., Tissot, P. E., Streich, M. M., Walker, J. S., Rubio, C., Amos, A. F., ... & Pasawicz, M. R. (2017). Hypothermic stunning of green sea turtles in a western Gulf of Mexico foraging habitat. *PloS one*, *12*(3), e0173920.

Suflita, J. M., Gibson, S. A., & Beeman, R. E. (1988). Anaerobic biotransformations of pollutant chemicals in aquifers. *Journal of industrial microbiology*, *3*(3), 179-194.

Rayson, M. D., Gross, E. S., Hetland, R. D., & Fringer, O. B. (2016). Time scales in Galveston Bay: An unsteady estuary. *Journal of Geophysical Research: Oceans*, *121*(4), 2268-2285.

Rhew, R. C., Miller, B. R., & Weiss, R. F. (2008). Chloroform, carbon tetrachloride and methyl chloroform fluxes in southern California ecosystems. *Atmospheric Environment*, *42*(30), 7135-7140.

Rigby, M., Park, S., Saito, T., Western, L. M., Redington, A. L., Fang, X., ... & Fraser, P. J. (2019). Increase in CFC-11 emissions from eastern China based on atmospheric observations. *Nature*, *569*(7757), 546-550.

Rontu Carlon, N., Papanastasiou, D. K., Fleming, E. L., Jackman, C. H., Newman, P. A., & Burkholder, J. B. (2010). UV absorption cross sections of nitrous oxide (N 2 O) and carbon tetrachloride (CCl 4) between 210 and 350 K and the atmospheric implications. *Atmospheric Chemistry and Physics*, *10*(13), 6137-6149.

Smith, L. A., Stock, T. H., Chung, K. C., Mukerjee, S., Liao, X. L., Stallings, C., & Afshar, M. (2007). Spatial analysis of volatile organic compounds from a community-based air toxics monitoring network in Deer Park, Texas, USA. *Environmental Monitoring and Assessment*, *128*(1-3), 369-379.

Tanhua, T., Fogelqvist, E., & Bastürk, Ö. (1996). Reduction of volatile halocarbons in anoxic seawater, results from a study in the Black Sea. *Marine Chemistry*, *54*(1-2), 159-170.

Tanhua, T., & Olsson, K. A. (2005). Removal and bioaccumulation of anthropogenic, halogenated transient tracers in an anoxic fjord. *Marine chemistry*, *94*(1-4), 27-41.

Temme, H. R., Carlson, A., & Novak, P. J. (2019). Presence, diversity, and enrichment of respiratory reductive dehalogenase and non-respiratory hydrolytic and oxidative dehalogenase genes in terrestrial environments. *Frontiers in microbiology*, *10*, 1258.

Tsai, T. T., Kao, C. M., & Hong, A. (2009). Treatment of tetrachloroethylene-contaminated groundwater by surfactant-enhanced persulfate/BOF slag oxidation—A laboratory feasibility study. *Journal of hazardous materials*, *171*(1-3), 571-576.

Schmalz, R. A. J. (2000). Demonstration of a nowcast/forecast system for Galveston Bay.

Sherry, D., McCulloch, A., Liang, Q., Reimann, S., & Newman, P. A. (2018). Current sources of carbon tetrachloride (CCl4) in our atmosphere. *Environmental Research Letters*, *13*(2), 024004.

Wallace, D. W., Beining, P., & Putzka, A. (1994). Carbon tetrachloride and chlorofluorocarbons in the South Atlantic Ocean, 19 S. *Journal of Geophysical Research: Oceans*, *99*(C4), 7803-7819.

Wanninkhof, R., Asher, W. E., Ho, D. T., Sweeney, C., & McGillis, W. R. (2009). Advances in quantifying air-sea gas exchange and environmental forcing.

Wanninkhof, R. (2014). Relationship between wind speed and gas exchange over the ocean revisited. *Limnology and Oceanography: Methods*, *12*(6), 351-362.

Warner, M. J., & Weiss, R. F. (1985). Solubilities of chlorofluorocarbons 11 and 12 in `water and seawater. *Deep Sea Research Part A. Oceanographic Research Papers*, *32*(12), 1485-1497.

Wittlingerová, Z., Macháčková, J., Petruželková, A., & Zimová, M. (2016). Occurrence of perchloroethylene in surface water and fish in a river ecosystem affected by

groundwater contamination. *Environmental Science and Pollution Research*, *23*(6), 5676-5692.

Vannelli, T. O. D. D., Logan, M. Y. K. E., Arciero, D. M., & Hooper, A. B. (1990). Degradation of halogenated aliphatic compounds by the ammonia-oxidizing bacterium Nitrosomonas europaea. *Applied and Environmental Microbiology*, *56*(4), 1169-1171.

Vollmer, M. K., Zhou, L. X., Greally, B. R., Henne, S., Yao, B., Reimann, S., ... & Zhang, F. (2009). Emissions of ozone-depleting halocarbons from China. *Geophysical research letters*, *36*(15).

Wang, J., Qin, P., & Sun, S. (2007). The flux of chloroform and tetrachloromethane along an elevational gradient of a coastal salt marsh, East China. *Environmental pollution*, *148*(1), 10-20.

WMO 1991 Scientific Assessment of Ozone Depletion: 1991, Global Ozone Research and Monitoring Project—Report No. 25 (Geneva, Switzerland: WMO) p 8.8

Yvon-Lewis, S. A., & Butler, J. H. (2002). Effect of oceanic uptake on atmospheric lifetimes of selected trace gases. *Journal of Geophysical Research: Atmospheres*, *107*(D20), ACH-1.

Zou, S., Stensel, H. D., & Ferguson, J. F. (2000). Carbon tetrachloride degradation: effect of microbial growth substrate and vitamin B12 content. *Environmental Science & Technology*, *34*(9), 1751-1757.

APPENDIX A

TABLES

Table A-1: Water Quality Data for March 2019 Cruise. N/D means no data.

Station	Longitude	Latitude	Salinity	Temp	DO	NO3	HPO4	HSiO3	NH4	NO2	Urea	PFBA	PFBS	PFOA	PFOS	6:2 FTS
				(°C)	(mM)	(μM)	(μM)	(μM)	(μM)	(μM)	(μM)	(ng/L)	(ng/L)	(ng/L)	(ng/L)	(ng/L)
1	-94.84	29.31	17.90	17.3	0.287	2.20	1.61	28.47	3.37	0.51	0.79	7.68	102.56	2.31	0.00	0.00
11	-94.80	29.38	19.99	18.3	0.360	1.47	2.24	31.63	1.08	0.68	0.65	12.34	405.76	2.67	0.00	0.00
3	-94.87	29.46	12.90	18.0	0.328	0.00	1.41	49.95	0.91	0.37	1.16	10.80	284.88	0.00	0.00	0.00
5	-94.78	29.45	12.89	18.0	0.305	0.00	1.24	35.41	0.99	0.36	0.81	14.10	677.40	3.09	0.00	0.00
14	-94.88	29.53	12.43	18.0	0.327	0.00	0.85	25.21	1.32	0.22	0.88	8.44	282.47	0.00	2.64	0.00
9	-94.75	29.71	1.46	17.7	0.309	36.43	1.07	95.48	2.08	0.23	1.08	8.51	280.11	2.29	0.00	0.00
12	-94.82	29.65	7.57	18.4	0.309	0.89	1.12	51.73	2.27	0.31	0.90	11.58	1878.54	3.98	0.00	0.00
13	-94.93	29.61	10.15	18.8	0.327	0.00	1.13	50.78	1.60	0.31	0.92	8.80	430.96	1.56	0.00	0.00
20	-95.05	29.73	7.53	18.3	0.250	78.24	4.45	69.95	5.17	2.34	1.49	23.62	470.48	21.39	434.47	6604.15
22	-95.02	29.70	9.32	18.4	0.279	53.25	3.16	76.65	4.38	1.54	1.21	12.07	643.96	12.98	123.43	2268.68
H1	-94.98	29.67	10.21	18.7	0.295	31.89	1.87	40.55	2.97	1.03	0.88	13.18	857.01	7.45	46.49	884.99

Table A-2: Water Quality Data for all June 2019 cruises**.** N/D means no data.

Station	Longitude	Latitude	Salinity	Temp	DO	NO3	HPO4	HSiO3	NH4	NO2	Urea	PFBA	PFBS	PFOA	PFOS	6:2 FTS
				(°C)	(mM)	(μM)	(μM)	(μM)	(μM)	(μM)	(μM)	(ng/L)	(ng/L)	(ng/L)	(ng/L)	(ng/L)
103	-95.00	29.46	0.29	28.8	0.187	0.41	5.91	142.57	1.47	0.10	0.33	5.02	45.01	1.66	2.13	0.00
101	-94.98	29.45	1.26	29.1	0.205	0.00	5.11	105.85	1.24	0.07	1.07	6.63	43.39	1.95	2.01	0.00
201	-95.09	29.75	5.94	29.5	0.138	80.79	10.17	108.21	8.22	13.15	1.52	6.03	47.23	1.48	2.22	0.00
202	-95.18	29.75	3.64	29.6	0.140	91.34	14.69	111.72	15.32	17.16	2.01	11.22	192.15	2.69	6.30	37.00
301	-95.09	29.80	1.91	30.1	0.191	69.20	8.05	99.97	4.61	2.98	0.47	48.25	182.77	10.64	25.55	136.55
302	-95.09	29.81	1.21	30.0	0.194	62.33	7.44	116.73	6.22	3.33	0.55	6.27	45.18	0.83	2.32	0.00
401	-94.70	29.50	6.55	28.5	0.206	8.63	2.16	101.00	1.41	0.40	0.44	10.06	52.06	2.17	4.48	32.01
402	-94.49	29.58	3.35	28.4	0.205	0.18	1.24	108.12	1.49	0.16	0.43	8.93	38.37	1.17	3.33	0.00
503	-94.75	29.83	0.15	28.7	0.193	18.88	1.99	104.12	1.77	0.13	0.79	5.17	29.04	1.37	2.01	0.00
502	-94.74	29.83	0.15	28.7	0.195	18.89	1.87	102.08	1.54	0.08	0.75	8.80	66.50	2.38	3.27	0.00
501	-94.73	29.80	0.15	28.6	0.192	19.97	1.78	101.55	1.55	0.10	0.65	4.16	48.42	0.89	3.12	0.00
1	-94.83	29.31	13.66	29.2	0.205	0.95	1.71	64.64	1.58	0.42	3.29	30.57	88.06	0.68	1.40	0.00
11	-94.80	29.38	20.80	28.7	0.185	2.11	1.16	14.34	1.27	0.60	2.11	23.89	74.94	0.00	0.00	0.00
3	-94.87	29.46	8.34	29.2	0.222	0.00	1.67	85.79	1.20	0.14	2.24	1.25	2.60	N/D	468.62	N/D
5B	-94.78	29.45	10.51	29.4	0.219	0.00	1.64	71.75	1.51	0.22	2.29	1.14	5.52	N/D	131.65	N/D
5A	-94.76	29.50	4.23	29.0	0.242	0.89	1.96	95.47	1.14	0.07	2.30	1.33	4.40	N/D	178.79	N/D
9	-94.75	29.71	0.16	29.6	0.259	0.72	1.00	101.69	1.45	0.08	1.12	1.45	1.73	6.22	45.17	18.32
12	-94.82	29.65	0.39	29.3	0.263	2.22	2.01	98.94	6.79	0.13	8.99	1.86	3.10	N/D	298.20	N/D
13	-94.93	29.61	1.80	29.4	0.270	0.07	2.52	110.53	1.48	0.02	2.31	1.47	2.93	N/D	294.06	N/D
20	-95.04	29.73	4.89	29.6	0.178	74.40	7.03	112.39	4.86	8.47	3.25	2.81	7.55	14.63	99.14	21.57

Table A-3: Water Quality Data for September 2019 Cruise. N/D means no data.

Station	Longitude	Latitude	Salinity	Temp	DO	NO3	HPO4	HSiO3	NH4	NO2	Urea	PFBA	PFBS	PFOA	PFOS	6:2 FTS
				(°C)	(mM)	(μM)	(μM)	(μM)	(μM)	(μM)	(μM)	(ng/L)	(ng/L)	(ng/L)	(ng/L)	(ng/L)
11	-94.80	29.38	17.16	28.8	0.221	2.05	2.27	44.90	2.86	0.95	1.44	3.91	11.00	0.00	0.00	0.00
5A	-94.76	29.50	7.96	28.4	0.193	0.59	1.39	39.32	1.79	0.25	1.57	2.21	10.28	0.72	1.38	0.00
14	-94.88	29.53	6.22	28.6	0.222	16.13	2.69	47.36	1.02	6.03	0.67	7.48	16.18	1.27	1.22	0.00
9	-94.75	29.71	1.23	28.9	0.239	5.78	1.48	61.08	2.41	0.13	1.22	1.53	13.03	0.00	0.86	0.00
12	-94.82	29.65	5.46	29.1	0.203	1.28	1.51	63.13	1.86	0.22	1.63	2.66	13.04	1.29	1.11	0.00
13	-94.93	29.61	4.82	29.0	0.295	6.73	2.06	49.78	3.20	4.14	3.21	3.84	15.44	1.03	1.23	0.00
20	-95.04	29.73	1.63	27.9	0.155	24.87	4.10	35.51	6.50	6.28	2.64	2.34	17.16	1.24	1.04	55.37
22	-95.02	29.70	2.04	28.7	0.194	17.93	3.46	56.66	3.52	3.59	0.83	3.05	20.10	1.05	0.99	26.39
H1	-94.98	29.67	3.16	28.5	0.139	20.33	3.46	48.40	4.38	5.45	1.08	1.82	9.13	1.02	1.40	32.36
3	-94.87	29.46	9.37	29.1	0.280	2.91	1.50	48.16	2.73	1.28	1.18	3.45	10.18	1.16	1.75	0.00

Table A-4: Water Quality Data for November 2019 Cruise. N/D means no data.

Station	Longitude	Latitude	Salinity	Temp	DO	NO3	HPO4	HSiO3	NH4	NO2	Urea	PFBA	PFBS	PFOA	PFOS	6:2 FTS
				(°C)	(mM)	(μM)	(μM)	(μM)	(μM)	(μM)	(μM)	(ng/L)	(ng/L)	(ng/L)	(ng/L)	(ng/L)
11	-94.80	29.38	17.98	11.7	0.304	2.03	2.07	56.62	3.43	0.48	1.22	N/D	N/D	N/D	N/D	N/D
5A	-94.78	29.47	13.25	11.1	0.314	2.92	2.28	43.71	2.52	0.73	0.94	N/D	N/D	N/D	N/D	N/D
14	-94.88	29.53	16.77	12.4	0.328	14.45	2.47	53.86	3.88	0.78	1.13	N/D	N/D	N/D	N/D	N/D
9	-94.76	29.71	10.48	11.8	0.380	5.73	1.72	64.77	3.40	0.23	0.53	N/D	N/D	N/D	N/D	N/D
12	-94.82	29.65	12.27	11.9	0.394	6.53	1.90	46.61	2.29	0.55	1.11	N/D	N/D	N/D	N/D	N/D
13	-94.93	29.61	13.88	13.3	0.309	52.98	4.18	47.29	10.29	1.84	1.14	N/D	N/D	N/D	N/D	N/D
20	-95.05	29.73	11.96	15.2	0.244	71.53	6.35	48.85	21.63	2.74	1.64	N/D	N/D	N/D	N/D	N/D
21	-95.02	29.72	11.11	15.0	0.264	64.44	6.37	45.01	16.65	2.68	1.39	N/D	N/D	N/D	N/D	N/D
22	-95.02	29.70	14.28	14.5	0.272	63.57	6.39	45.85	17.09	2.78	1.47	N/D	N/D	N/D	N/D	N/D
H1	-94.98	29.67	16.81	13.2	0.275	40.75	4.22	58.52	11.17	1.71	1.32	N/D	N/D	N/D	N/D	N/D
3	-94.87	29.46	15.33	14.4	0.333	7.37	2.33	50.86	2.49	0.61	1.09	N/D	N/D	N/D	N/D	N/D

Table A-5: Spearman values for March 2019 Cruise**.** Bold Values signify p < 0.05

	CCl4	CFC-11	CHCl3	PCE	Temp	Salinity	DO	NO3	HPO4	HSiO3	NH4	NO2	Urea	PFBA	PFBS	PFOA	PFOS	6:2 FTS†
CCl4	-	-	-	-	-0.155	-0.245	**-0.781**	**0.837**	**0.718**	0.382	**0.664**	**0.774**	0.436	0.391	0.064	**0.656**	**0.611**	0.786
CFC-11	**0.609**	-	-	-	0.255	-0.364	**-0.854**	**0.651**	0.564	0.364	**0.873**	**0.610**	0.291	0.282	0.327	**0.761**	0.400	0.619
CHCl3	0.355	0.536	-	-	**0.691**	-0.518	-0.562	0.321	0.364	0.391	0.591	0.433	**0.655**	0.400	0.564	0.542	**0.779**	0.786
PCE	0.527	0.409	**0.818**	-	0.509	**-0.709**	-0.470	0.535	0.355	**0.718**	0.539	0.433	**0.845**	0.473	0.536	0.579	**0.695**	0.786

†: Only three datapoints with values above 0

Table A-6: Spearman values for all June 2019 Cruises**.** Bold Values signify p < 0.05

	CCl4	CFC-11	CHCl3	PCE	Temp	Salinity	DO	NO3	HPO4	HSiO3	NH4	NO2	Urea	PFBA	PFBS	PFOA	PFOS	6:2 FTS†
CCl4	-	-	-	-	**0.580**	0.285	-0.363	0.194	0.215	0.182	0.218	**0.553**	-0.006	-0.062	0.020	**0.536**	0.068	0.572
CFC-11	0.329	-	-	-	**0.622**	0.280	**0.461**	-0.277	0.095	-0.107	-0.054	-0.029	**0.533**	**-0.611**	**-0.617**	**0.561**	**0.786**	0.612
CHCl3	**0.793**	**0.764**	-	-	**0.842**	-0.143	-0.491	**0.636**	**0.804**	**0.554**	**0.700**	0.458	0.125	-0.211	0.011	**0.554**	0.414	0.450
PCE	**0.560**	0.538	0.484	-	0.420	0.282	-0.254	**0.742**	**0.566**	0.159	**0.747**	**0.798**	0.055	0.313	0.297	0.335	**0.566**	0.546

†: Only three datapoints with values above 0

Table A-7: Spearman values for September 2019 Cruise**.** Bold Values signify p < 0.05

	CCl4	CFC-11	CHCl3	PCE	Temp	Salinity	DO	NO3	HPO4	HSiO3	NH4	NO2	Urea	PFBA	PFBS	PFOA	PFOS	6:2 FTS†
CCl4	-	-	-	-	N/D	N/D	N/D	N/D	N/D	N/D	N/D	N/D	N/D	N/D	N/D	N/D	N/D	N/D
CFC-11	N/D	-	-	-	**-0.867**	-0.212	**-0.818**	0.600	**0.742**	-0.539	0.527	**0.697**	-0.091	-0.103	0.248	0.116	0.055	0.813
CHCl3	N/D	0.600	-	-	-0.321	-0.539	-0.309	**0.927**	**0.863**	-0.030	**0.648**	**0.818**	-0.212	0.055	0.527	0.511	0.079	0.798
PCE	N/D	0.527	**0.673**	-	-0.442	**-0.685**	-0.491	**0.782**	**0.790**	0.018	**0.673**	0.406	-0.212	-0.248	0.442	0.000	-0.539	0.798

†: Only three datapoints with values above 0

Table A-8: Spearman values for November 2019 Cruise**.** Bold Values signify p < 0.05

	CCl4	CFC-11	CHCl3	PCE	Temp	Salinity	DO	NO3	HPO4	HSiO3	NH4	NO2	Urea	PFBA	PFBS	PFOA	PFOS	6:2 FTS
CCl4	-	-	-	-	**0.664**	-0.273	**-0.791**	**0.809**	**0.718**	0.018	**0.918**	**0.709**	**0.791**	N/D	N/D	N/D	N/D	N/D
CFC-11	0.455	-	-	-	0.118	0.073	**-0.736**	0.173	0.373	-0.200	0.555	0.336	**0.664**	N/D	N/D	N/D	N/D	N/D
CHCl3	**0.864**	0.273	-	-	**0.900**	-0.200	**-0.709**	**0.973**	**0.855**	-0.182	**0.836**	**0.855**	**0.836**	N/D	N/D	N/D	N/D	N/D
PCE	**0.673**	0.582	**0.700**	-	0.573	0.136	**-0.782**	0.591	**0.664**	-0.127	**0.655**	0.600	**0.864**	N/D	N/D	N/D	N/D	N/D